Title

Operando Investigation of the Molecular Origins of Dipole Switching in P(VDF-TrFE-CFE) Terpolymer for Large Adiabatic Temperature Change

Authors

Zhu, Yuan
Wu, Hanxiang
Martin, Andrew
et al.

Publication Date

2024

DOI

10.1002/adfm.202314705

Operando Investigation of the Molecular Origins of Dipole Switching in P(VDF-TrFE-CFE) Terpolymer for Large Adiabatic Temperature Change

*Yuan Zhu[†1], Hanxiang Wu[†1], Andrew Martin[2], Paige Beck[2], Elshad Allahyarov[3, 4, 5], Thumawadee Wongwirat[3], Guanchun Rui[3], Yingke Zhu[1], Daniel Hawthorne[2], Jiacheng Fan[1], Jianghan Wu[1], Siyu Zhang[1], Lei Zhu[*3], Sumanjeet Kaur[*2], and Qibing Pei[*1]*

Yuan Zhu, Hanxiang Wu, Yingke Zhu, Jiacheng Fan, Jianghan Wu, Siyu Zhang, Qibing Pei
[1]Department of Materials Sciences and Engineering, Henry Samueli School of Engineering and Applied Science, University of California, Los Angeles, California 90095, USA.
E-mail: qpei@seas.ucla.edu

Andrew Martin, Paige Beck, Daniel Hawthorne, Sumanjeet Kaur
[2]Energy Storage and Distributed Resources Division, Lawrence Berkeley National Laboratory, Berkeley, CA, 94720, USA.
E-mail: skaur1@lbl.gov

Elshad Allahyarov, Thumawadee Wongwirat, Guanchun Rui, Lei Zhu
[3]Department of Macromolecular Science and Engineering, Case Western Reserve University, Cleveland, Ohio 44106-7202, USA.
E-mail: lxz121@case.edu

Elshad Allahyarov
[4]Institut für Theoretische Physik II: Weiche Materie, Heinrich-Heine Universität Düsseldorf, 40225 Düsseldorf, Germany.
[5]Theoretical Department, Joint Institute for High Temperatures, RAS, 125412 Moscow, Russia.

[†]These authors contributed equally to this work.

Keywords: electrocaloric cooling effect, P(VDF-TrFE-CFE) terpolymer, operando investigation, dipole switching

Relaxor ferroelectric polymers exhibiting a giant electrocaloric effect (ECE) can potentially be used to create next-generation solid-state coolers. Under an electric field, poly(vinylidene fluoride-trifluoroethylene-chlorofluoroethylene) terpolymer goes through a large dipolar entropy change producing a high adiabatic temperature change (ΔT_{ECE}). This work resolves the molecular origins of the large entropy change behind the electric field-induced dipole switching. A Fourier transform infrared spectroscopy equipped with a high voltage source was used to operandoly observe the characteristic molecular vibrational modes. We discovered that a short-range trans (T) conformation of the CF_2-CH_2 dyads interrupted by a gauche (G) conformation, *e.g.*, TTTG in the terpolymer chain, undergoes a dynamic transformation that leads to a corresponding ΔT_{ECE} whenever an electric field was applied. The molecular dynamics simulation also proved that the energy barrier that the transformation from TTTGs into a long T sequence overcomes is smaller than that for all other conformations. We employed a mixed solvent system to obtain T3G-enriched terpolymer films exhibiting a 4.02 K ΔT_{ECE} at 60 MV m^{-1} and used these films to manufacture a 2-layer-cascaded cooling device that achieved a 6.7 K temperature lift, the highest reported value for a 2-layer cascaded device made of fluoropolymers.

1. Introduction

Relaxor ferroelectric polymers exhibiting large reversible polarization change have shown promise to enable future solid-state refrigeration. An electric field applied across such a dielectric polymer film can lead to a large entropy change and thus a large adiabatic temperature change in the material. [1] This electrocaloric effect (ECE) has been utilized for pumping heat in cooling devices.[2] The potential advantages that such polymer-based ECE coolers offer include avoidance of potent greenhouse gas-generating refrigerants, high coefficient of performance (COP), and compact and flexible form factors.[3-5] However, the ability to effectively realize all of these advantages depends heavily on being able to further enhance the terpolymer's adiabatic temperature change (ΔT_{ECE}), particularly at a consistent and sustainable electric field strength of approximately 50-60 MV m^{-1}. In addition, fabricating the coolers also requires a scalable process for creating polymer films with relaxor ferroelectric microstructures that can then produce the required large ΔT_{ECE}.

Poly(vinylidene fluoride-trifluoroethylene-chlorofluoroethylene) terpolymer, P(VDF-TrFE-CFE), is a widely investigated relaxor ferroelectric polymer material. The chlorine atom in the

CFE monomer is believed to be responsible for breaking the long-range ordering of the polymer chains, expanding the inter-chain distance, and thus lowering the energy barrier of dipole switching, such that the switching may be dynamically obtained with an intermediate applied electric field at room temperature. [6, 7] Different models have been proposed to explain the mechanism of this switchable polarization. Zhang et al. originally proposed that the field-induced nonpolar-to-polar phase transformation generates a large dipolar entropy change (ΔS_{dip}) and a high ΔT_{ECE}.[8, 9] Qian et al. put forward the idea that a large number of polar entities arranged in a disordered manner with smaller crystallites and larger interfacial areas can result in a large ΔS_{dip}.[7] However, the specific molecular structural units that are directly responsible for the large ΔS_{dip} still remain elusive. Being able to properly understand and clarify this elusive aspect is imperative for the design of novel molecular structures and film microstructures that can further enhance ΔT_{ECE} and assist in developing of a scalable fabrication process.

PVDF-based ferroelectric and relaxor ferroelectric polymers have been known to have different crystalline polymorphs, *e.g.*, the β-phase that has long range *trans* (T) conformation of the CF_2-CH_2 dyads, the α-phase with long range alternating *trans* and *gauche* (G) or TGTG', and the γ-phase which is the intermediate between the α- and the β-phase and takes on TTTGTTTG' conformation (**Figure 1**(a) to (c)). The G' indicates a slight C─C bond rotation that minimizes the systematic energy for close stacking.[10] The β-phase is ferroelectric while the α-phase is paraelectric, and the γ-phase is in between the two. The P(VDF-TrFE-CFE) terpolymer, when at a typical composition of 65/35/7 mol% (the total amount of the VDF and the TrFE monomer is regarded as being 100%), is unlikely to have long range Ts or TGs. Therefore, it is more logical to describe the dyad arrangements with the T and G sequences rather than the α-, β- and γ-phases. The T dyads carry dipole moments perpendicular to the polymer chains, and a long T sequence is highly polar, while TGTG' is non-polar.[11] The TTTG conformation, also noted as T3G, has a 50% polarization as compared to a long T sequence.[11] These different conformations may respond differently to an applied electric field and thus exhibit disparate ECEs.

Fourier transform infrared (FTIR) spectroscopy has been shown to be a simple and useful technique for identifying the molecular conformations within the terpolymer.[12] For instance, the relative weak absorptions at 772 and 800 cm^{-1} are due to the bending and rocking modes of T3G,[13] and the bending of the long T sequence occurs at 1287 cm^{-1}.[14]

The use of operando measurements for analyzing the FTIR spectra of a P(VDF-TrFE-CFE) film under an applied electric field holds the potential to provide unprecedented and valuable insights into the molecular conformations that are being altered, or polarized, by the electric field. Through carefully monitoring the dynamic changes that occur in the spectra as the field strength ramps up, one may unravel the nature of the switching dipoles responsible for the giant ECE. When these operando measurements of FTIR are supplemented by molecular dynamics (MD) simulation and other experimental techniques such as X-ray diffraction (XRD) and differential scanning calorimetry (DSC), they might collectively provide an unambiguous understanding of the electrocaloric mechanisms that are at play in the relaxor ferroelectric fluoropolymers. Furthermore, considering that the terpolymer films' microstructures are highly influenced by various processing conditions, it becomes evident that a holistic approach is necessary to not only enhance their ECE, but also ensure high reproducibility and scalability, which are essential attributes for the fabrication of high-performance cooling devices.

2. Results and Discussion

In thin film fabrication, the terpolymer solidifies on the substrate either from a solution or a melt. Due to the high polarity of the C-F bonds, the terpolymer is soluble in highly polar organic solvents, such as N,N-Dimethylformamide (DMF) and Dimethyl sulfoxide (DMSO). If the terpolymer is dissolved in DMF, which has a 3.8 D dipole moment at 20 ºC [15] and a 153 ºC boiling point, the solvent will evaporate almost completely at 55 ºC in 12 hours after drop-casting. This is a traditional way to fabricate terpolymer thin films and the film is named S1 film. We also used DMSO to partially replace DMF since DMSO has a higher dipole moment (4.1D at 20 ºC) [15] and boiling point (189 ºC). We tried a number of DMF:DMSO combinations, and found that films (named S2 film) formed from DMF:DMSO (1:1 in volumetric ratio) solution at 70 ºC exhibit good evenness and improvement in ΔT_{ECE}. DMSO portion greater than 50% led to solution viscosity being too high for drop-casting uniform films. Similarly, terpolymer thin films can be fabricated via the melt-and-quench method. The S1 film was first heated to 135 ºC for 1.5 hours to melt the terpolymer and thus its microstructures formed during DMF evaporation were erased. Then we quenched the molten terpolymer in 20 ºC room temperature water to freeze the microstructures. This film is called S1-MQ film. Finally, we put half of the films processed from each casting method to an overnight high temperature treatment in vacuum at 115 ºC to investigate the annealing effect

on the film microstructures, and named them S1-A, S2-A and S1-MQ-A film, respectively. A summary of nomenclature and the fabrication processes of the six types of films can be found in Table 1.

Table 1. Fabrication methods and conditions of terpolymer film samples.

Name	Fabrication Processes
S1	Cast from DMF solution at 55 °C
S1-A	S1, annealed at 115 °C for 16 h
S2	Cast from DMF:DMSO (1:1) solution at 70 °C
S2-A	S2, annealed at 115 °C for 16 h
S1-MQ	S1, heated at 135 °C (above T_m) for 1.5 h and then quenched in 20 °C water for 1 min
S1-MQ-A	S1-MQ, annealed at 115 °C for 16 h

These different processing methods provide a wide range of thermodynamic or kinetical conditions and thus lead to various molecular microstructures (conformations and morphologies) within the terpolymer films. While some microstructures contribute to a high ΔS_{dip} and ΔT_{ECE} upon the application of an electric field, others may have less effect. The optical photographs of the six different films are shown in Figure 1(d). All films have good quality and uniform thickness, which is essential for thin film device applications. These high-quality films show large variations in opaqueness, indicative of their different microstructures. ΔT_{ECE}s of the films were directly measured with an IR camera. For an accurate temperature sensing, the tested area on each film was suspended in air to prevent rapid heat loss from thermal conduction. In addition, the IR camera was set to have a default emissivity (ε) value of 0.98. Figure 1(e) presents the representative ΔT_{ECE}s of the different terpolymer films. The ΔT_{ECE} at each field strength was calculated based on the average temperature values of five samples processed with each method, and the measurement was taken during the first electric field ramping-up procedure from 20 to 80 MV m^{-1} with an increment of 10 MV m^{-1}. For the unannealed films formed from solvent evaporation, the S2 film has about 20% increase in ΔT_{ECE} throughout the electric field range compared to the S1 film. Vacuum annealing at 115 ºC has significantly enhanced the ΔT_{ECE}, as S1's ΔT_{ECE} is increased from 2.25 to 3.66 K in S1-A at 60 MV m^{-1}, and S2's ΔT_{ECE} is increased from 2.64 to 4.03 K in S2-A at 60 MV m^{-1}. The annealing has the largest effect on the S1-MQ film, increasing its ΔT_{ECE} from 0.36 to

1.96 K in S1-MQ-A at 60 MV m^{-1}. Overall, the S2-A film shows the highest ΔT_{ECE} of 4.03 K at 60 MV m^{-1} and the S1-MQ film has the lowest ΔT_{ECE} of 0.36 K at 60 MV m^{-1}.

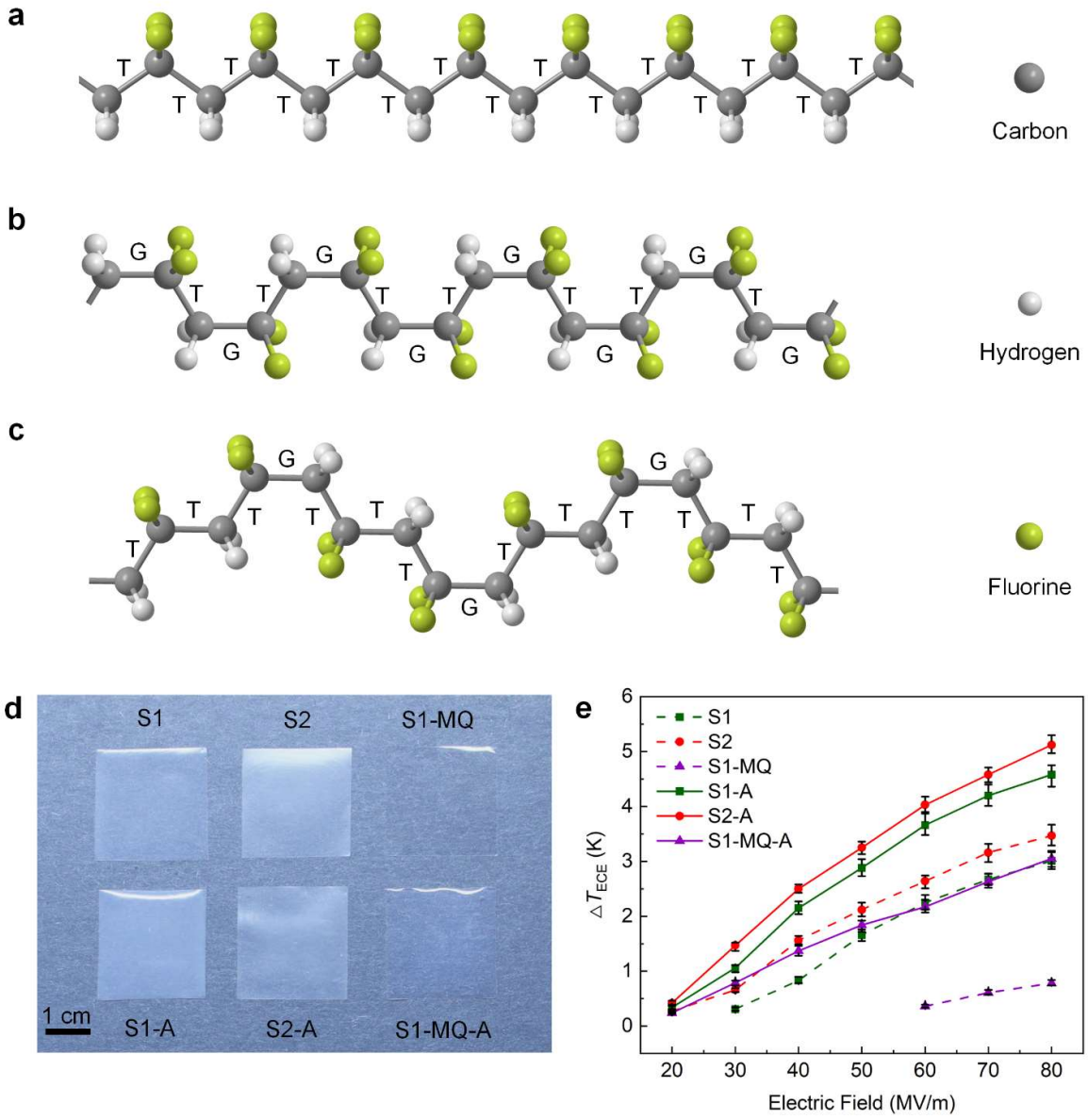

Figure 1. (**a**) β-like long T sequence. (**b**) α-like TGTG' sequence. (**c**) γ-like TTTGTTTG' sequence. (**d**) Optical photographs of terpolymer films fabricated using various methods. (**e**) ΔT_{ECE}s of the terpolymer films as the electrical field was increased from 20 to 80 MV m^{-1}. The ΔT_{ECE} of the S1-MQ film at fields below 60 MV m^{-1} are undistinguishable due to a low signal-noise ratio.

Infrared spectroscopy has been used to characterize the trans and gauche conformations of fluoropolymers.[16] We coupled an FTIR machine with a high-voltage source to study the conformational change when an electric field was applied across the terpolymer films (**Figure**

S1). Absorbance FTIR spectra were recorded by scanning the full spectral range for 32 scans to guarantee the steadiness of the vibrational peaks. **Figure 2** gives the FTIR spectra of the samples with no electric field applied. In the wavenumber range of 1600-400 cm^{-1}, large differences in peak intensities among the six samples are observed at 1287, 848, 772, 800 cm^{-1} and at a doublet band at 605/614 cm^{-1}. The untruncated FTIR data can be found in **Figure S2**(a). To show the reproducibility of the fabrication, the FTIR spectra of 3 samples for each of the S1-A film and the S2-A films are shown in Figure S2(b) and (c). The FTIR data shows conformity among the samples, indicating that the analysis lays on reliable ground, and the reproducibility of the fabrication process is good. In the following passage, we will discuss what those bands represent and how they can be utilized to characterize the dipole switching in the terpolymer under an electric field.

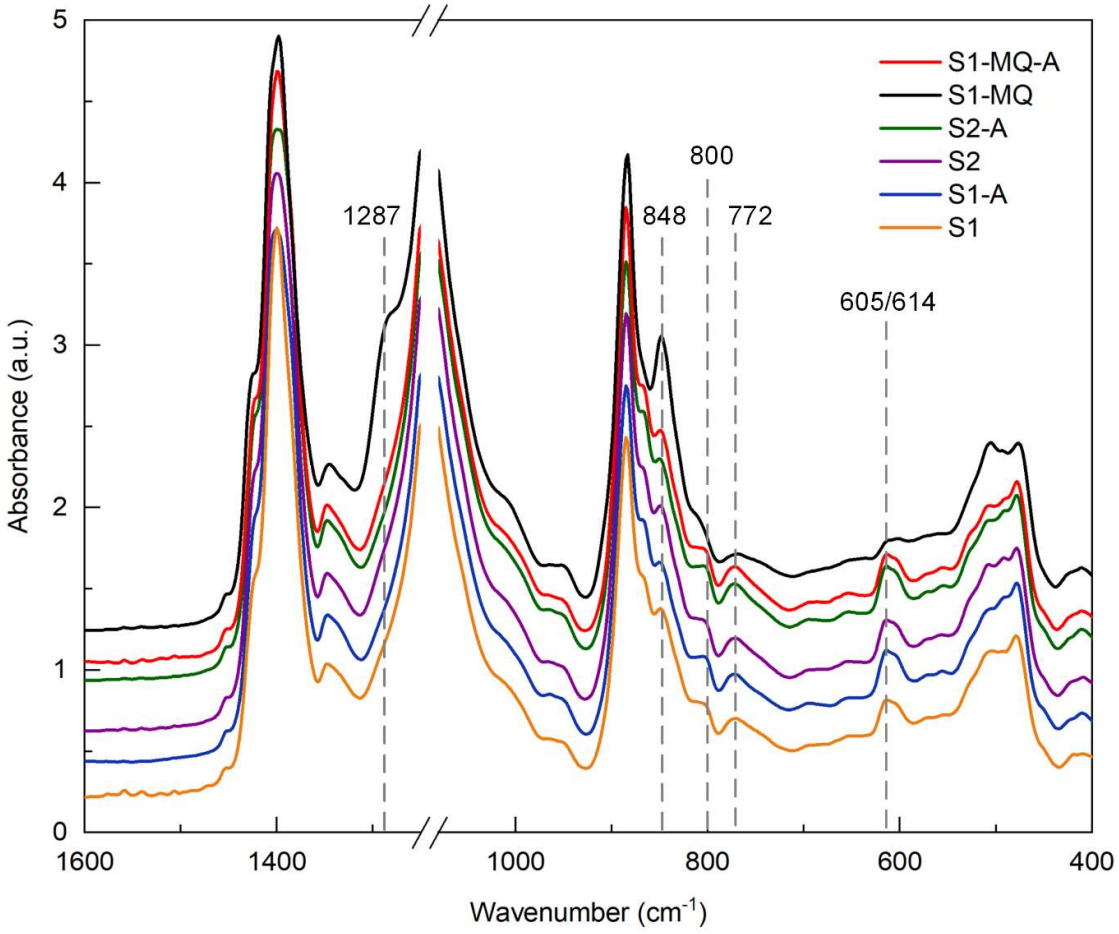

Figure 2. FTIR spectra of terpolymer films without electric field. Curves are elevated sequentially by 0.5 units in the vertical direction for easy reading purpose. The signals from 1080 to 1250 cm^{-1} showed no clear patterns and were too high, so they were cut out from the plot.

Figure 3 presents the operando FTIR spectra of the S1-A film, which is made with a traditional method and exhibits a large ΔT_{ECE} at 60 MV m^{-1}. As the electric field is increased from 0 to 60 MV m^{-1}, the two bands at 772 and 800 cm^{-1}, which are assigned to T3G conformations [13], become much weaker at higher field strengths. Meanwhile, bands at 848 and 1287 cm^{-1} arise and intensify progressively as the electric field strength increases. These two bands are assigned to the long T sequences (T>3 and T>4, respectively).[14, 17] There is also a doublet band at 605/614 cm^{-1} that decreases in intensity as the electric field ramps up. According to literatures, a sharp or intense peak at 614 cm^{-1} is observed and assigned to the *α*-phase PVDF with regular TGTG' conformation [13, 18], and the 605 cm^{-1} peak might be assigned to the amorphous PVDF with random TG conformation.[17] In the P(VDF-TrFE) copolymer, a broad peak in the 605-614 cm^{-1} range is observed and attributed to the TG and TG' units (TGs) in short trans sequences (e.g., TTGTTT isomers) [18-20], while this peak can also contain some of TGTG' sequences. The doublet peak observed here in the S1-A terpolymer film sample is also weak and diffusive. Therefore, we speculate that when an electric field is applied, bond rotations mostly take place at or near the short T sequences, *e.g.*, T3G. The bond rotations coincide with or lead to realignment of dipoles with the electric field. When the 60 MV m^{-1} electric field is removed, the FTIR spectrum returns back to the starting spectrum (see **Figure S3**(a)), indicating that this dipole switching is fully reversible. In other words, S1-A exhibits relaxor ferroelectric behavior at the applied electric field range at room temperature.

More details can be found if we look closely at the bands at 605/614, 772, 800 cm^{-1} that lower in intensity when an external field is present. These bands all have specific vibrational assignment of the TGT segment.[13] As the field increases, the TGT segments of T3G sequences become much less, and the long T sequences (bands at 848 and 1287 cm^{-1}) become noticeable. This observation prompts us to propose a mechanism of dipole switching in which the G conformation vanishes and a long T sequence is formed. When the external field is applied, dipoles of T3 in T3G tend to be aligned with the field, and the three Ts will be switched as an entity. In this way, the G conformation disappears as its two adjacent T3s get aligned to form a longer-range all T conformation (**Figure 4**). Consequently, the bands at 848 and 1287 cm^{-1} are enhanced. Note that these field-induced long T sequences are different from the long T sequences in the crystalline β phase of PVDF (Figure 1(a)), as the bond angles are squeezed due to the limited local chain mobility (Figure 4). The squeezed long T

sequences are not thermodynamically favorable and can be formed only when the electric field is applied. When the electric field is revoked, they will relax back to the original T3G sequences. We speculate that T sequences shorter than T3Gs may have lower electrostriction force to overcome energy required for the G to T transformation, while T sequences longer than T3Gs incur greater chain movement for the transformation. Thus, T3G represents the optimal molecular conformation to achieve reversible polarization and accessible entropy change with an electric field.

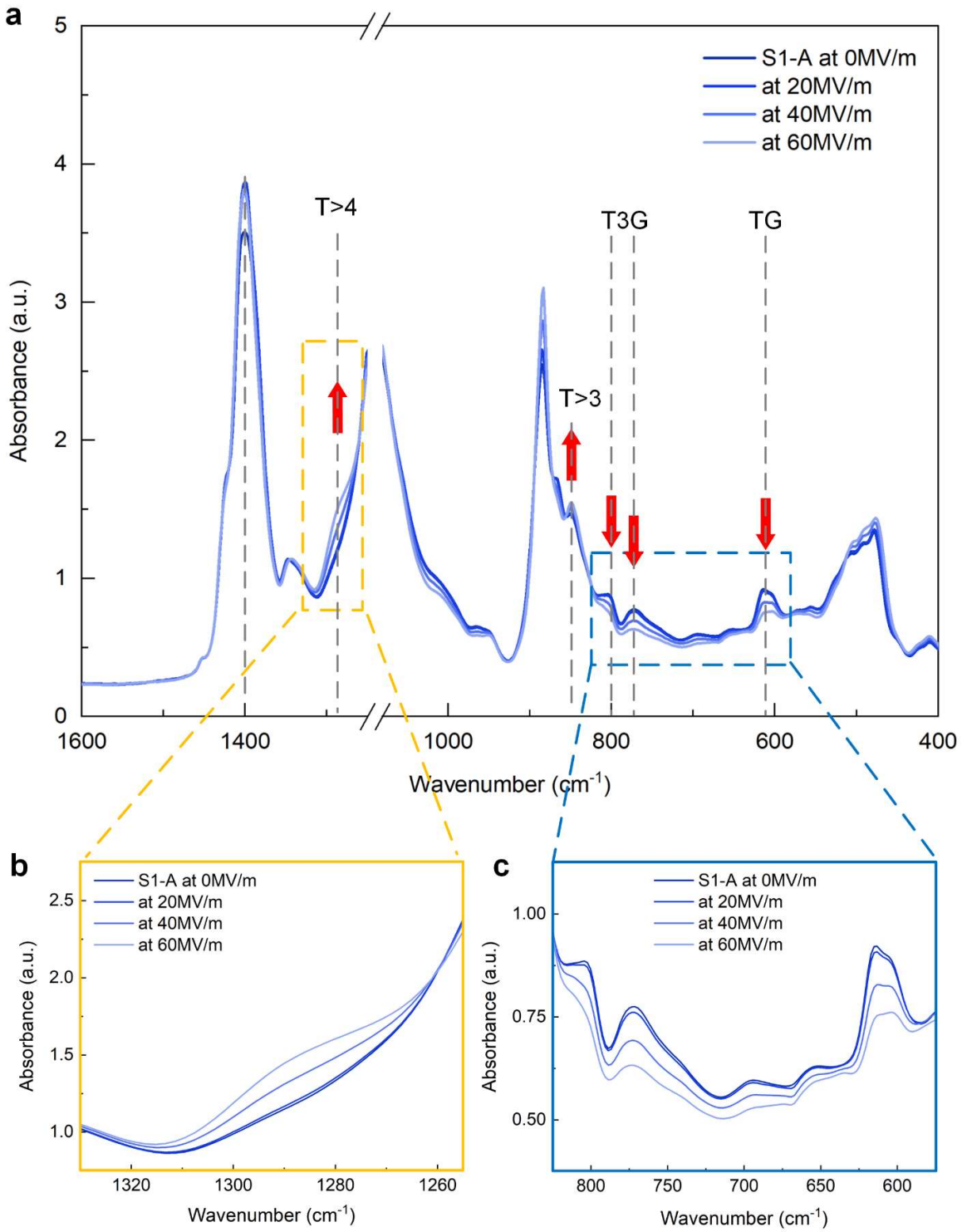

Figure 3. (**a**) FTIR spectral evolution of an S1-A film as the electric filed is increased from 0 to 60 MV m^{-1}. The red arrows show the trends of change of the characteristic peaks as the electric field ramps up (lighter color indicates higher field). The detailed views of the spectral change are shown for long T sequences (**b**) and for T3G and TGs in short T sequences characteristic peaks (**c**).

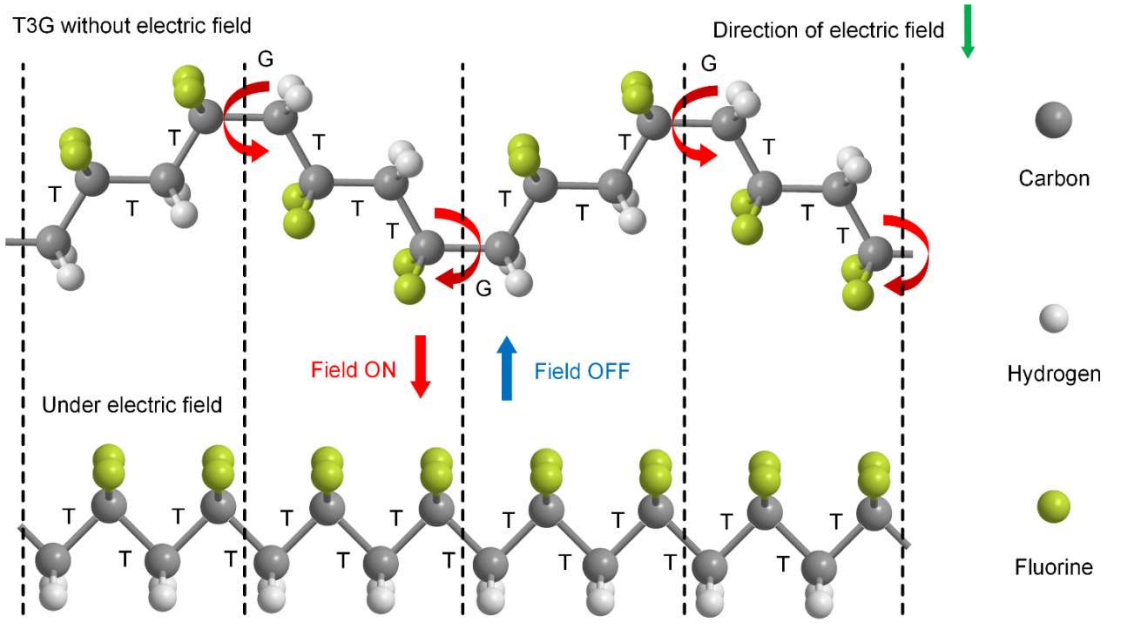

Figure 4. Proposed dipole switching mechanism involving G-to-T transformation as adjacent T3Gs merge into one squeezed long T sequence. Only the molecular units of VDF are shown in the diagram for simplicity.

We performed molecular dynamics (MD) simulation to compare the ease of transformation from different conformations to long T sequences. Four characteristic conformations of a $H_3CCF_2(CH_2CF_2)_{14}CH_3$ chain in vacuum were examined: long T sequence $TTT(TTTT)_6TTT$, γ-like chain $TTT(TTTG)_6TTT$, α-and-γ mixed chain $TTT[(TTTG)(TGTG')]_3TTT$, and α-like chain $TTT(TGTG')_6TTT$ (**Figure S4**(a)-(d)). The Coulomb **(**U_{coul}), bond (U_{bond}), angle (U_{angle}) and torsional ($U_{torsion}$) energies were calculated per atom. These energies, the total energy per atom ($U_{per\text{-}atom}$), and the per-atom energy differences ($\Delta U_{per\text{-}atom}$) between the characteristic conformation chains and the long T chain are presented in Table S1. More details about the simulation method can be found in Supporting Information Section 1. The energy difference (ΔU_{unit}) of each repeat unit (e.g., TTTG, TGTG' and [TTTG/TGTG']/2) which contains 4 carbon-carbon bonds between the γ, α-and-γ mixed, and α conformation and the long T sequence is 0.876 eV, 0.960 eV, and 1.008 eV, respectively (Table S1). This result shows that the transformation from the γ conformation to the long T sequence has the lowest energy barrier, in consistent with the argument that the T3G-to-T4 transition is predominant in the ECE of the P(VDF-TrFE-CFE) terpolymer at low fields.

For tracking the transformation from the initial α, γ, and α+γ chains to the β chain, additional MD simulations were carried out under a poling field E = 100 MV m^{-1}. The field, applied perpendicular to the chain length, tries to orient the entire chain along its direction. In order to suppress this movement and keep the chain orient perpendicular to the applied field, we fixed the x and z coordinates of the chain-end atoms to their initial positions while allowing them to slide along the y-axis, which is the axis along the chain length. Such sliding opportunity for the poled chain is necessary to accommodate the longer β chain length. In Figure S4(e)-(g), we present representative two-dimensional (2D) snapshots from the poling simulations. In Figures S4h and S4i, we present the dipole moment and potential energy changes of the chains during poling.

Similar to the short T sequences, the long T sequences are also electrically active but have larger polarization. Re-orienting such large dipoles at a high electric field could lead to giant polarization, which may be responsible for the ferroelectric behavior of PVDF and P(VDF-TrFE) copolymers. However, as their small interchain distances and large domain sizes limit the mobility, the polarization-field curve shows large hysteresis. Furthermore, the reorientation of polar domains does not significantly contribute to entropy change [7,9], only leading to small ΔS_{dip} and thus low ΔT_{ECE} values. In contrast, the reorientation of the short T sequences, *e.g.*, T3G, can produce non-polar to polar phase change [7] and thus generate a large ΔS_{dip} and high ΔT_{ECE}. More importantly, the transformation incurs only a small chain movement, given that the electrocaloric effect is reversible. When the field is removed, a large cooling ΔT_{ECE} is obtained in a short timeframe.

In contrast to S1-A, the S1-MQ films have almost negligible ΔT_{ECE} (0.36 K at 60 MV m^{-1}). In **Figure 5**, the FTIR spectrum of this film at 0 MV m^{-1} shows prominent peaks at 848 and 1287 cm^{-1}, signifying that there is a large amount of long T sequences in the film. Nevertheless, bands at 772 cm^{-1} and 800 cm^{-1}, which are assigned to T3G are inconspicuous. The doublet peak at 605/614 cm^{-1} is also very flat. As the electric field is increased from 0 MV m^{-1} to 60 MV m^{-1}, the bands assigned to T3G do not show large intensity reduction (Figure 5d). Interestingly, the bands at 848 cm^{-1} and 1287 cm^{-1} show a small decrease in intensity as the electric field ramps up (Figures 5(b) and (c)). We speculate that this small loss takes place when the long T sequences re-align with the electric field. Unfortunately, the entropy change associated with the reorientation of long T sequence is quite small and the S1-MQ film only exhibits a low ΔT_{ECE}.

Since the sample was melt quenched and was highly transparent, one may consider it largely amorphous. However, as Table S2 shows, S1-MQ's fusion enthalpy (15.10 J g^{-1}) is comparable to that of S1 (14.17 J g^{-1}), at the same melting point of 127-128 ºC (**Figure S5**). Therefore, the S1-MQ film has a same level of crystallinity as the S1 film does. For the S1 and S2 films, annealing at a high temperature increases the crystallinity and the ΔT_{ECE} is improved in proportion. However, for the S1-MQ film, annealing makes its ΔT_{ECE} surge (increased for 6 times) with only 19% increase in crystallinity. The reason will be explained below, and this phenomenon indicates that crystallinity does not absolutely correlate to the ΔT_{ECE} of the terpolymer.

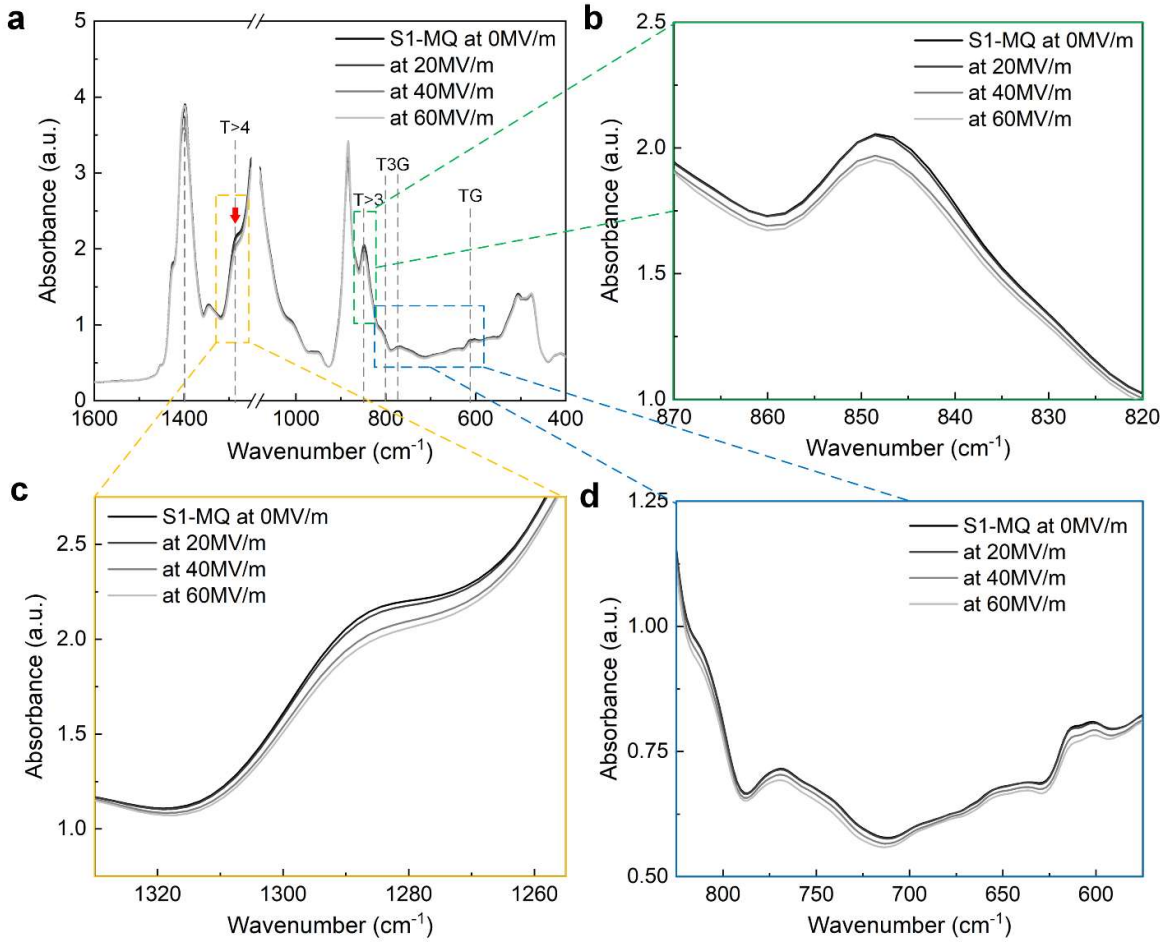

Figure 5. (**a**) FTIR spectral evolution of an S1-MQ film as the electric filed is increased from 0 to 60 MV m^{-1}. Detailed views of the spectral changes of long T sequences (T>3) around 848 cm^{-1} (**b**), long T sequences (T>4) around 1287 cm^{-1} (**c**) and T3G at 772 and 800 cm^{-1} and TGs in short T sequences around 605/614 cm^{-1} (**d**).

XRD was used to further examine the microstructures of the terpolymer films prepared under different conditions. **Figure 6**(a) shows the XRD patterns of the S1 and S1-A films. Both films show a main peak at 18.4º of 2θ, which corresponds to the paraelectric phase (TG, T3G, and other short T sequences) [21] of PVDF-based polymer crystals with a 4.8 Å inter-chain spacing (Table S3). S1 film spectrum has a shoulder peak at 19.3º, which has been attributed to the ferroelectric phase (long T sequences) in PVDF-based polymers [16] with a smaller inter-chain spacing of 4.6 Å (Table S3). The XRD patterns of S1-MQ and S1-MQ-A are shown in Figure 6(b) where the spectrum curve position and shape of S1-MQ-A are similar to those of S1-A except for a barely recognizable diffraction at 19.3º. Nonetheless, the XRD spectrum of the S1-MQ film is rather diffusive. We deconvolute the diffusive XRD peak of S1-MQ into two Gaussian peaks at 18.4º and 19.3º, respectively (**Figure S6**). The paraelectric and ferroelectric peaks have comparable but low signal intensities. The paraelectric peak might come from the small amount of TGTG' inside the irregular crystallites within the S1-MQ film. However, the majority of TGTG' is not able to contribute to a large ΔS_{dip} or ΔT_{ECE} at electric fields below 50-60 MV m^{-1}. An earlier study has shown that even at a much higher field (up to 125 MV m^{-1}), there was no conformational change from TGTG' to a long T sequence as T3G does.[22]

The overnight annealing at 115 ºC increases the S1-MQ film's ΔT_{ECE} from 0.36 K to 1.95 K in S1-MQ-A at 60 MV m^{-1}, a 6-fold increase. For the PVDF-based polymers, annealing at a temperature between the recrystallization point (~108 ºC shown in Figure S5) and the melting point (~128 ºC shown in Figure S5) not only increases the crystallinity, but also transforms a part of the long T sequences into TG and short T sequences. This is shown in Figure 2 where the FTIR peaks of long T sequences at 850 and 1287 cm^{-1} disappear and the T3G peaks show up after the S1-MQ film is annealed. In Figure 6(b), the disappearance of the ferroelectric peak at 19.3º and the emergence of a sharp peak at 18.4º also reveal that the transformation from long T sequences to short T sequences and TGs are quite substantial during the annealing process.

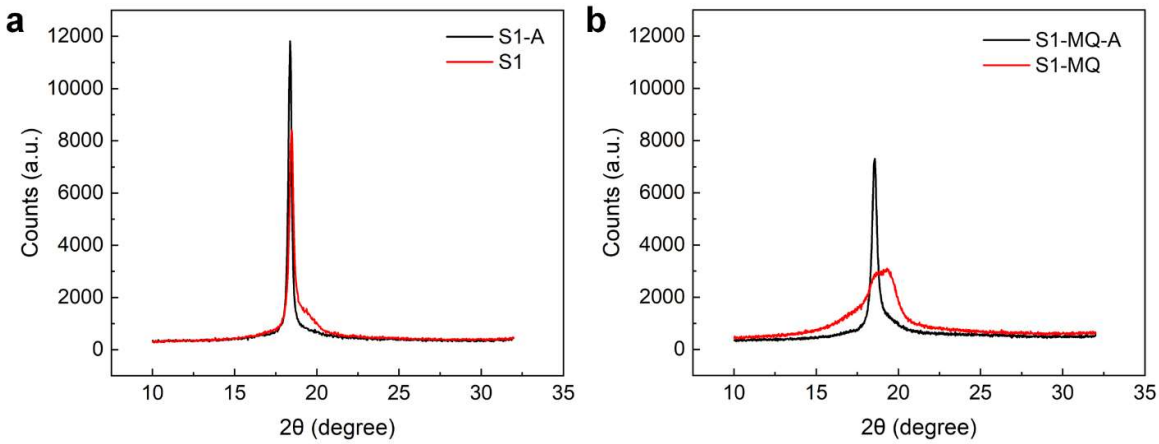

Figure 6. XRD spectra of the S1 and S1-A films (**a**) and the S1-MQ and S1-MQ-A films (**b**).

Among the short T sequences, T3G seems to have the proper balance of electrostriction force and chain mobility for the G to T transformation under an electric field. Enhancing the electrocaloric performance of the terpolymer would hinge on increasing the abundance of T3G in the processed films. Therefore, we used DMSO to partially replace DMF in the casting solution. DMSO has a higher melting point than DMF. As the solvent evaporates, the terpolymer chains are surrounded by the remaining DMSO molecules which have a higher molecular dipole moment. The interactions between the terpolymer and the polar solvent promote the uncoiling of the terpolymer chains, and encourage the formation of the more polar trans segments.[15] It is worth mentioning that the casting temperature should be increased if a solvent with a higher boiling point is used to avoid the formation of excessive long T sequences [16], and only facilitate the growth of short T sequences. Therefore, the drying temperature of S2 films with DMSO:DMF (1:1) solvent used was elevated to the optimized 70 ºC (compared to 55 ºC when DMF was used). Excessive long T sequences do not significantly contribute to ΔT_{ECE}, and the high temperature annealing cannot fully transform the long T sequences due to a memory effect, which will be elucidated in the end of this section.

The exothermal peak at 35-42 °C on the DSC spectrum provides additional evidence about whether the casting temperature is proper for the restrained growth of the long T sequences. This enthalpy involved corresponds to the transition from the metastable all trans phase to the paraelectric phase of PVDF-based polymers.[16, 23] In the terpolymer, this is the transformation from long T sequences to TG and short T sequences (Figure S5), and the peak area correlates to the amount of the long T sequences in the freshly cast films. The S2* film cast at 55 °C

shows a larger peak area compared to the S2 film cast at 70 °C, signifying that 70 °C can better prevent the growth of excessive long T sequences. On the other hand, elevating the casting temperature above 70 °C will have an adverse effect since the solvent's polarity decreases substantially at high temperature.[16]

Based on T3G and other short T sequences being the main molecular units contributing to ΔS_{dip}, we performed a quantitative analysis of the T3G/short Ts peak areas on the FTIR spectra of each kind of the terpolymer film. **Figure 7**(a) shows the FTIR spectra of the S1 and the S2 films at 0 and 60 MV m^{-1} for comparison and illustration purposes. The FTIR spectra of the two films have similar shapes and curvatures but different peak intensities at the same electric field. The expanded views of the spectrum of the S2 film at 0 MV m^{-1} are displayed in Figures 7(b) and (c) to show the tangent lines that define the peaks. The peak areas were computed using simple numerical integration, and then were normalized to the area of the steady peak at 1400 cm^{-1} of the film to correct any small but inevitable thickness variations among different samples. Finally, this method was employed to all the six different types of films. Table 2 presents the summations of the normalized areas of the peaks at 605/614, 772 and 800 cm^{-1}, and also the variations (reductions) in the total peak area when the electric field was increased from 0 to 60 MV m^{-1}. Additionally, the relationship of ΔT_{ECE} against the variation in the total peak area is plotted in Figure 7(d). From Table 2 and Figure 7(d) we can see that generally, a film with a larger total T3G/short Ts peak area has a larger variation in this total area when a field is applied, and the film also exhibits a higher ΔT_{ECE} (i.e., the S2-A film has the largest total peak area of 17.6 cm^{-1} and the highest ΔT_{ECE} of 4.03 K at 60 MV m^{-1} as well). Figure 7(d) even clearly demonstrates a notable linear relationship between ΔT_{ECE} and the variation in the total peak area when an electric field is applied. These phenomena further substantiate that the electrocaloric change in the terpolymer originates from the short T sequences, and our strategy of adding DMSO to the casting solvent can help promote short T sequences to form. For additional information of the champion S2-A film, its operando FTIR spectra is shown in **Figure S7**, and the XRD spectra of both the S2-A and the S2 films are shown in **Figure S8**.

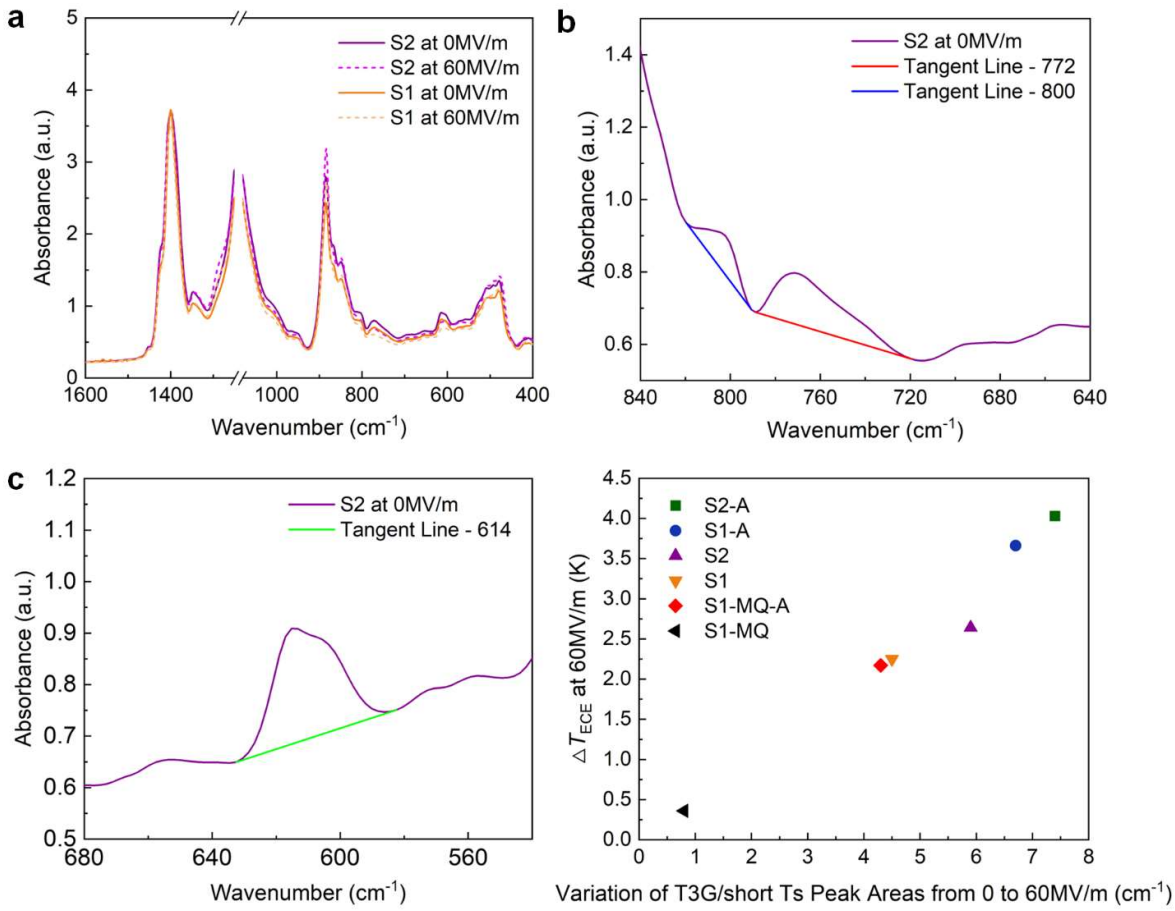

Figure 7. (**a**) FTIR spectra of the S1 and the S2 films at 0 and 60 MV m^{-1}. Expanded views of the spectrum of the S2 film at 0 MV m^{-1} for its peaks at 772 and 800 cm^{-1} (**b**) and the peak at 605/614 cm^{-1} (**c**) with tangent lines defining the peaks. (**d**) The ΔT_{ECE} at 60 MV m^{-1} versus the variation in the total T3G/Short Ts peak area when the field is increased from 0 to 60 MV m^{-1}.

Table 2. Total T3G/short Ts peak areas (summation of the peaks areas at 605/614, 772, and 800 cm^{-1}) of the terpolymer films and the reductions in the total areas when a 60 MV m^{-1} electric field is applied.

Film Type	**Total T3G/short Ts Peak Area at 0 MV m^{-1} (cm^{-1})**	**Variation in Total T3G/short Ts Peak Area from 0 to 60 MV m^{-1} (cm^{-1})**	**ΔT_{ECE} at 60 MV m^{-1} (K)**
S2-A	17.6	7.4	4.03
S1-A	16.6	6.7	3.66

S2	15.9	5.9	2.64
S1	14.2	4.5	2.25
S1-MQ-A	15.7	4.3	2.17
S1-MQ	9.3	0.8	0.36

Annealing at 115 °C can improve the ΔT_{ECE}s of the S1, S1-MQ, and S2 films. Nonetheless, the annealed films do exhibit significantly different ΔT_{ECE}, which may be due to the so-called memory effect of fluoropolymers where part of the ordered structures can endure and serve as nuclei for subsequent crystallite growth during annealing or melting.[24, 25] In other words, the abundant fraction of T3G in the freshly cast S2 films was retained during high temperature annealing, and they could even encourage the growth of more T3G conformations. Overall, the initial microstructures of the terpolymer produce certain ΔT_{ECE} based on the solvent polarity and drying temperature. Subsequent treatments can further modify the microstructures and the resulting ΔT_{ECE}s. In the terpolymer, at room temperature, the T3G conformation which contributes to high ΔT_{ECE} is a metastable state, whereas the TG conformation is the more stable, low-polarity state, and the long T sequences are highly polar and metastable given the presence of CFE units in the polymer chains.

Finally, the dynamic dielectric properties are studied with broadband dielectric spectroscopy (BDS). **Figure S9** gives the BDS-tested real and imaginary relative permittivity as a function of temperature at different frequencies for the six films. The broad peaks of the dielectric permittivity, located at T_m, of all the films except the S1-MQ film, shift to lower temperatures as the probing field frequency decreases, a generic feature of relaxor ferroelectric materials. On the contrary, the locations of the dielectric permittivity peaks of the S1-MQ film concentrate at 40 °C. This is the Curie transition (T_C) of the ferroelectric phase formed within the film and is consistent with the DSC result in Figure S5(b). In Figure S9(b), T_C is observed to be at 12 °C for the S2-A film at 10Hz, well below that of the S1-MQ film and further confirming that the terpolymer is a relaxor ferroelectric at room temperature after proper processing. The ferroelectric behavior of the six different films was studied with the displacement-electric field (D-E) (**Figure S10**(a)-(f)) and the current-electric field (I-E) loop (Figure S10(g)-(l)) measurements at 1Hz. The I-E loop of S1-MQ (Figure S10(l)) film exhibits simple reversal response and thus the ferroelectric nature. I-E loops of the other five films show complex patterns as the electric field changes, signifying that the relaxor ferroelectric phase dominates within these films. Compared to the unannealed films, the

annealed films show more closed D-E loops, indicating that annealing can effectively transfer the remaining ferroelectric phase (long T sequences) into paraelectric phase. The S2-A film with the highest ΔT_{ECE} exhibits the narrowest and the most obvious double hysteresis D-E loop (DHL). DHLs are frequently obtained from the relaxor ferroelectric P(VDF-TrFE-CFE) due to the weak pinning effect of the CFE monomer. [26] When the polling field is high, the DHL resembles ferroelectric behavior as long T sequences are formed. When the field goes back to a much lower level, the loop has little remnant polarization and is similar to a paraelectric behavior.

Utilizing the S2-A films, we fabricated a solid-state cooling device that was shown in **Figure 8**(a). The device had a two-stack cascade structure. Each stack comprised two S2-A films spray coated with CNT electrodes and laminated together.[4] When a square-wave electric field (0 and 60 MV m^{-1}) was applied at 1 Hz, the cascade device with a thermal laminate in between the two S2-A stacks can potentially achieve a temperature lift (ΔT_{Device}) nearly twice of the material's ΔT_{ECE}. Figure 8b shows the transient temperature at the cold and the hot sides of the device measured with an infrared camera. The temperatures reached steady values at 18.8 °C and 25.5 °C, respectively, after about 30 seconds of operation. The ΔT_{Device} is 6.7 K, which is 170% that of the material ΔT_{ECE} at the same field. It is also higher than the record ΔT_{Device} we previously reported for a 2-layer cascade device (5.5 K). [4]

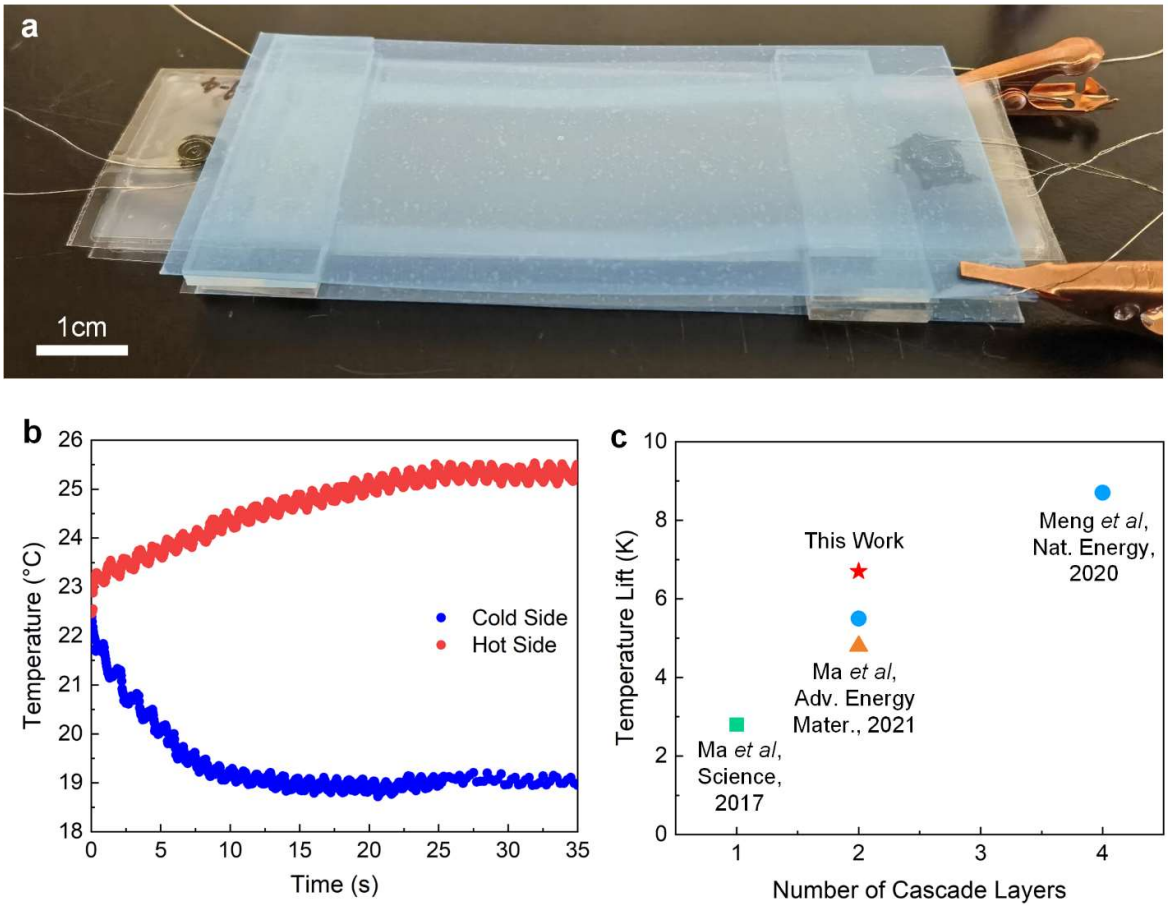

Figure 8. (**a**) Top-view photo of a 2-layer cascade electrocaloric cooling device. (**b**) The temperature profile on the cold and the hot side of a 2-layer cascade electrocaloric cooling device operating with two double-layer S2-A terpolymer films. (**c**) The temperature lift value compassions among different ECE cooling devices made with fluoropolymer stacks.

3. Conclusion

The operando FTIR offers a direct observation of the dipole switching phenomenon, which is the underlying mechanism that drives the notable entropy and temperature changes in the terpolymer when subjected to an electric field. When the transformation from G to T takes place, two adjacent T3Gs converge into a long T sequence that aligns with the electric field. Due to the chain mobility being restricted, this long T sequence is squeezed when compared to the long T sequences within a regular β-phase PVDF. When the field is revoked, the molecular stress drives the relaxation of the squeezed long T sequence back into T3Gs. The MD simulation result also reveals that under an electric field, the transformation from T3Gs to long T sequences has the lowest energy barrier compared to that of transformations that occur in other conformations. The reversible reorientation of the T3G units contributes to the large

ΔS_{dip} and the large ΔT_{ECE}. With this knowledge in mind, we used a high-polarity solvent DMSO to enrich the T3G content. The ΔT_{ECE}s of both the unannealed and annealed terpolymer films were accordingly enhanced by casting them using a solvent containing DMSO. This dual solvent strategy can also be more broadly and effortlessly applied when fabricating terpolymer films with larger areas and different thicknesses. Thermal annealing provides an additional means to manipulate the microstructures because the annealing process transforms the long T sequences into short T sequences, helping to enhance the ΔT_{ECE}s. Finally, we demonstrated how this all can work by constructing a cascaded solid-state cooler based on the S2-A films which translated the improved material ΔT_{ECE} into a device's higher temperature lift.

The low intensity of the T3G peaks on the FTIR spectra indicated that only a small portion of the terpolymer was in fact present in the T3G conformation, and that there may be a lot of room for further boosting the ΔT_{ECE}s. Gaining a deeper understanding of how the amorphous regions, and the interfaces between the crystalline and the amorphous regions, aid the dipole switching may offer new insights into the ECE mechanism. In addition, the vast array of available solvents and solvent mixtures, along with diverse annealing temperatures and durations, presents a rich field for exploration to enhance the ΔT_{ECE}. Further improvements in the material ΔT_{ECE}s and the device structures will help pave the way for the realization of the high-performance solid-state cooling devices that can make good use of soft materials.

4. Experimental Section

Materials

P(VDF-TrFE-CFE) (65/35/7 mol%, the total amount of the VDF and the TrFE monomer is regarded as 100%) terpolymer (batch #64-018) was purchased from Piezotech. P3-CNT was purchased from Carbon Solutions, Inc. N, N-Dimethylformamide was purchased from Supelco, Inc. Dimethyl sulfoxide was purchased from VWR International. PTFE syringe filter was purchased from Millipore Sigma. Quartz substrate, steel shim, and polyester (PET) film are purchased from McMaster-Carr. Cyanoacrylate glue was purchased from Gluemasters. All materials were used as received unless otherwise specified.

Equipment

The infrared (IR) camera has a brand and a model number of ICI 9320p. The high voltage box is from Trek 609E-6 high voltage amplifier. The portable high voltage box is from Poly-K

Technologies, LLC with a 10 kV/2 mA HV DC power supply. The DSC is from TA Instruments with a model name of DSC2500. The XRD is from PANalytical X'Pert Pro X-ray Powder Diffractometer. The FTIR machine is the Cary 660 FTIR Spectrometer from Agilent Technologies.

Preparation of Terpolymer Films and Post Treatments

For the preparation of films used for adiabatic temperature change measurement, 1 g of P(VDF-TrFE-CFE) terpolymer was dissolved in 8.5 ml solvent (DMF for sample S1 or DMF:DMSO (Dimethyl sulfoxide) (1:1 in volumetric ratio) for sample S2), and stirred overnight at room temperature. The resulting solution was filtered through a syringe filter with 0.2μm pore size. The filtered solution was then drop cast onto a 10 ×10 cm^2 quartz substrate and dried overnight at 55 °C for S1 films and 70 °C for the S2 films. The S2* film was dried at 55 °C with the DMF:DMSO(1:1) solvent. These films had a thickness of 50 μm. The films were then heated at 90 °C for 1h to remove residual solvents. For the preparation of films used for the FTIR characterization, 0.63 g of the terpolymer was dissolved in 8.5 ml solvent and all the other operations are the same as in the preparation of S1 and S2 films. The resulting FTIR films had a thickness of 30 μm.

Selected films cast from the DMF solution were heated to 135 °C for 1.5 h and then quenched in room temperature deionized water for 1 min. These films were called melt quenched films or S1-MQ.

For films that needed to be annealed, annealing was typically done in a vacuum oven at 115 ±1 °C for about 16 h.

To apply the electrodes, the films were covered by a contact mask with the 16 electrode patterns, followed by spray-coating of a carbon nanotube (CNT) dispersion in solvent at a 0.5 mg mL^{-1} concentration until the sheet resistance reached 10 kΩ. The carbon nanotube dispersion was prepared by mixing 10 mg P3-CNT with 18ml of isopropanol and 2ml of water. The dispersion was sonicated for 50 h and centrifuged at 8000 rpm for 15 min to collect the supernatant for spray coating. The 10 × 10 cm^2 terpolymer film was then peeled off from the substrate and cut into 16 2.5 × 2.5 cm^2 small films after the electrode application. Then they were aligned to the mask and spray-coated on the back side.

Measurement of adiabatic temperature change

The 2.5 cm × 2.5 cm × 50 μm terpolymer film with CNT electrodes on both sides was clamped and suspended horizontally above the benchtop. An IR camera was positioned right

above the film surface by 25 cm. The defaulted infrared emissivity of 0.98 was used for temperature measurement by assuming that the existence of the CNT electrodes did not cause any infrared to be reflected back to the polymer film and thus could not be captured by the IR camera. As a result, our ΔT_{ECE} values are modest measurements. If a ΔT_{ECE} was measured with an emissivity lower than the actual value, ΔT_{ECE} would be mistakenly overestimated. For ΔT_{ECE} measurement details, electric fields ranging from 1 to 4 kV with a 0.5 kV increment were applied across the films with square waves that had a 50% duty cycle and lasted 10 seconds in total. Three cycles of each electric field strength were applied to the film to collect three ΔT_{ECE} data points for the calculation of the average value. Transient temperature profile was measured in real-time. Finally, the temperature change when the voltage was turned off was noted as the ΔT_{ECE} during cooling.

Operando FTIR measurement

Terpolymer films used for operando FTIR scanning were 30 μm in thickness, thinner than the films used for ΔT_{ECE} measurement which were rather too thick to obtain accurate FTIR spectra. The 2.5 cm × 2.5 cm × 30 μm terpolymer films with CNT electrodes coated on both sides were connected to the test leads via insulating high-voltage cables and mounted to the sample holder within the chamber of the FTIR machine. The cables reaching out from the FTIR machine were connected to a portable high voltage box. Constant voltages ranging from 0 to 1.8 kV with an increment of 0.6 kV were applied across the film via the CNT electrodes. At each voltage level, 32 scans were taken by the FTIR machine, and this process took about 20 to 30 seconds to complete.

DSC Measurement

The DSC equipment is from TA Instruments with a model name of DSC2500. The ramp rate is 5°C min^{-1}. The pan type is Tzero Alod Aluminum Hermetic with a cylindrical shape and an internal volume of 40μL. The sample pan and lid are Tzero Alodined Pans and Tzero Hermetic Alodined Lids (with a TA instruments part numbers of 901697.901 and 901698.901 respectively). The sample mass is around 5mg for each run.

XRD Measurement

X-ray diffraction (XRD, X'Pert Pro, PANalytical) in the 2θ range of 10°-32° with Cu anode/Kα (λ = 0.15406 nm) radiation was used to characterize the terpolymer films.

Molecular Dynamic (MD) Simulation

A full atomistic MD simulation was carried out for a single chain in the vacuum. Four conformations were implemented: TTT(TTTT)$_6$TTT, γ-like T$_3$(T$_3$GT$_3$G')$_3$T$_3$, α-and-γ mixed T$_3$[(T$_3$G)(TGTG')]$_3$T$_3$, and α-like T$_3$(TGTG')$_6$T$_3$; see Figure S4(a)-(d) in SI for illustration. Each chain consisted of 31 carbon atoms, 34 H, and 30 F atoms, so there were in total 95 atoms within one molecular chain (neglecting two hydrogens at each end of the chain). Each chain contained a TTT conformation at both ends. All chains were created using the Avogadro2 software and equilibrated in the MD simulation before calculating their energy. All hydrogen, fluorine, and carbon atoms were treated as van der Waals (vdW) monomers with partial electrostatic charges for the carbon atom in the CH_2 group: $q_{C(H)}$ = -0.5202e, for the carbon atom in the CF_2 group: $q_{C(F)}$ = 0.6120e, q_H = 0.1807e, and q_F = -0.2266e located at the atomic centers. Two end carbon atoms had 3 H atoms with a slightly modified charge. The hydrogens at the one end of the chain had q_H = 0.12e, whereas at the other end of the chain q_H = 0.173e, which guaranteed full electroneutrality of the chain. The monomers of the same chain interacted with each other through the specific two-body bond-stretching potential U_{bond}, three-body angle-bending potential U_{angle}, and four-body dihedral angle bending potential $U_{dihedral}$. These potentials and other details of the MD simulations are available in pages 14 and 15 of the supporting information of this reference publication.[27]

The permittivity of the medium ε_r = 1 as a chain is in vacuum. The simulation box size was 12×12×12 nm, and the chain was placed in the middle of the box and oriented along the *y*-axis. The polymer chain was immobilized, and its total energy was calculated as a sum of its bond, angular, torsional, and electrostatic energies. The calculated data is given in Table S1. MD runs with a Langevin thermostat with a friction coefficient γ = 2 ps^{-1} and a Gaussian white-noise force of strength $6k_BT\gamma$ was performed in a constant NVT ensemble. The equations of motion were integrated using the velocity Verlet algorithm with a time step of 1 fs. We imposed standard periodic boundary conditions by filling the space with translational replicas of the fundamental cell in the *x* and *y* directions. During the initial stage of the simulation, the system is gradually raised from zero to room temperature in 6 consecutive runs at increments of 50 K. In each run the system is equilibrated for 20 ps. Once the system temperature reaches 300 K, simulation data, such as the positions of atoms, their velocities, and the forces acting on them, are stored at time intervals of 1 ps for processing later.

We performed fully atomistic simulations by treating the hydrogen, fluorine and carbon atoms of the PVDF as van der Waals (vdW) monomers with their partial electrostatic charges located at the atomic centers. The total potential energy of the system is given as:

$$U_{total} = U_{vdW} + U_q + U_{bond} + U_{angle} + U_{dihedral} \quad (1)$$

Here, the first two terms on the right-hand side are pair interactions between non-bonded atoms. The first term is the van der Waals interaction:

$$U_{vdW}(r) = \sum_{i>j} A_{ij} e^{-B_{ij} r_{ij}} - \frac{C_{ij}}{r_{ij}} \quad (2)$$

where $r$ij is the separation distance between the atoms i and j, and Aij, Bij and Cij are atom type specific parameters.

The second term is the electrostatic interaction potential:

$$U_q = \sum_{i>j} \frac{q_i q_j e^2}{\varepsilon(r_{ij}) r_{ij}} \quad (3)$$

where ql(l = i or j) is the atomic partial charge. The last three terms on the right side of **Equation 1** represent the potential energy of the bonded segments of the chains. The two-body bond-stretching potential is defined as:

$$U_{bond}(R) = \frac{1}{2} \sum_{all\ bonds} k_b (R - R_0)^2 \quad (4)$$

and it has a simple Hookean form with stretching constant kb and unstretched bond length R0. For the three-body angle-bending potential we use:

$$U_{angle}(\theta) = \frac{1}{2} \sum_{all\ bond\ pairs} k_\theta (\theta - \theta_0)^2 \quad (5)$$

where θ_0 is an equilibrium bending angle and $k\theta$ is a bending force constant. Finally, the dihedral (four-body) component of the total energy is written as:

$$U_{dihedral}(\varphi) = \frac{1}{2} \sum_n \sum_{all\ bonds\ triplets} k_\varphi(n)[1 - \cos(n\varphi)] \quad (6)$$

In **Eqations 4-6**, all the two-body, three-body, and the four-body interaction constants depend on the type of the atoms involved in the interaction. These parameters, as well as the van der Waals interaction parameters and the atomic partial charges, were taken from the force-field developed by Byutner and Smith for PVDF polymers.[28]

Molecular dynamics (MD) runs with a Langevin thermostat with a friction coefficient $\gamma = 2$ ps^{-1} and a Gaussian white-noise force of strength $6k_BT\gamma$ were performed for the β-form PVDF crystal for time periods up to 500 ps in a constant NVT ensemble. The equations of motion were integrated using the velocity Verlet algorithm with a time step of 1 fs. We imposed standard periodic boundary conditions by filling space with translational replicas of the fundamental cell in the *x* and *y* directions.

Supporting Information

Supporting Information is available from the Wiley Online Library or from the author.

Data Availability Statement

Original data can be obtained from the corresponding authors upon reasonable request.

Competing Interests

The authors declare no competing interests.

Acknowledgements

The authors acknowledge partial finance support by the Office of Naval Research (award no. N00014-19-1-2212), and the use of instruments at the cleanroom of California NanoSystems Institute (CNSI) and the UCLA Molecular Instrumentation Center. E.A. and L.Z. acknowledge financial support by the National Science Foundation, Division of Materials Research, Polymers Program (DMR-2103196). This work was supported by the Laboratory Directed Research and Development Program (LDRD) at Lawrence Berkeley National Laboratory under contract # DE-AC02-05CH11231. Yuan Zhu and Hanxiang Wu contributed equally to this work.

Received: ((will be filled in by the editorial staff))
Revised: ((will be filled in by the editorial staff))
Published online: ((will be filled in by the editorial staff))

References

[1] Z. Kutnjak, B. Rožič, R. Pirc, *Wiley Encyclopedia of Electrical and Electronics Engineering*, **2015**, 1-19.

[2] Y. Meng, J. Pu, Q. Pei, *Joule*. **2021**, *5*, 780.

[3] R. Ma, Z. Zhang, K. Tong, D. Huber, R. Kornbluh, Y. S. Ju, Q. Pei, *Science.* **2017**, *357*, 1130.

[4] Y. Meng, Z. Zhang, H. Wu, R. Wu, J. Wu, H. Wang, Q. Pei, *Nat Energy.* **2020**, *5*, 996.

[5] X. Chen, W. Zhu, A. S. Rattner, Q. M. Zhang, *J. Phys. Energy.* **2023**, *5*, 024009.

[6] R. J. Klein, F. Xia, Q. M. Zhang, F. *Bauer, Journal of Applied Physics.* **2005**, *97*, 094105.

[7] X. Qian, D. Han, L. Zheng, J. Chen, M. Tyagi, Q. Li, F. Du, S. Zheng, X. Huang, S. Zhang, J. Shi, H. Huang, X. Shi, J. Chen, H. Qin, J. Bernholc, X. Chen, L. -Q. Chen, L. Hong, Q. M. Zhang, *Nature.* **2021**, *600*, 664.

[8] Q. M. Zhang, V. Bharti, X. Zhao, *Science*. **1998**, *280*, 2101.

[9] B. Neese, B. Chu, S. -G. Lu, Y. Wang, E. Furman, Q. M. Zhang, *Science.* **2008**, *321*, 821.

[10] T. Furukawa, *Phase Transitions.* **1989**, *18*, 143.

[11] N. A. Shepelin, A. M. Glushenkov, V. C. Lussini, P. J. Fox, G. W. Dicinoski, J. G. Shapter, A. V. Ellis, *Energy Environ. Sci.* **2019**, *12*, 1143.

[12] L. Yang, X. Li, E. Allahyarov, P. L. Taylor, Q. M. Zhang, L. Zhu, *Polymer.* **2013**, *54*, 1709.

[13] M. A. Bachmann, W. L. Gordon, J. L. Koenig, J. B. Lando, *Journal of Applied Physics.* **1979**, *50*, 6106.

[14] K. Tashiro, M. Kobayashi, H. Tadokoro, *Macromolecules.* **1981**, *14*, 1757.

[15] G. Knotts, A. Bhaumik, K. Ghosh, S. Guha, *Applied Physics Letters.* **2014**, *104*, 233301.

[16] H. -M. Bao, J. -F. Song, J. Zhang, Q. -D. Shen, C. -Z. Yang, Q. M. Zhang, *Macromolecules.* **2007**, *40*, 2371.

[17] M. Kobayashi, K. Tashiro, H. Tadokoro, *Macromolecules.* **1975**, *8*, 158.

[18] K. J. Kim, N. M. Reynolds, S. L. Hsu, *Macromolecules.* **1989**, *22*, 4395.

[19] K. Tashiro, K. Takano, M. Kobayashi, Y. Chatani, H. Tadokoro, *Polymer.* **1981**, *22*, 1312.

[20] K. Tashiro, M. Kobayashi, *Polymer.* **1988**, *29*, 426.

[21] N. Jia, Q. He, J. Sun, G. Xia, R. Song, *Polymer Testing.* **2017**, *57*, 302.

[22] G. T. Davis, J. E. McKinney, M. G. Broadhurst, S. C. Roth, *Journal of Applied Physics.* **2008**, *49*, 4998.

[23] Y. Liu, G. Zhang, A. Haibibu, Z. Han, Q. Wang, *Journal of Applied Physics.* **2019**, *126*, 234102.

[24] H. Pan, B. Na, R. Lv, C. Li, J. Zhu, Z. Yu, *Journal of Polymer Science Part B: Polymer Physics.* **2012**, *50*, 1433.

[25] S. Schneider, X. Drujon, B. Lotz, J. C. Wittmann, *Polymer*. **2001**, *42*, 8787.

[26] Z. Zhang, M. H. Litt, and L. Zhu, *Macromolecules*. **2017**, *50*, 5816.

[27] Y. Huang, G. Rui, Q. Li, E. Allahyarov, R. Li, M. Fukuto, G. -J. Zhong, J. -Z Xu, Z. -M. Li, P. L. Taylor, L. Zhu, *Nat. Commun*. **2021**, *12*, 675.

[28] O. G. Byutner, G. D. Smith, *Macromolecules.* **2000**, *33*, 4264.

The dynamic dipole switching situation in the relaxor ferroelectric P(VDF-TrFE-CFE) terpolymer under an externally applied electric field is studied with operando Fourier transform infrared. Short trans sequences (T3G) along the polymer chains are found to be responsible for the large entropy and the adiabatic temperature change since they can be actively flipped by the external field.

Yuan Zhu[†1], Hanxiang Wu[†1], Andrew Martin[2], Paige Beck[2], Elshad Allahyarov[3, 4, 5], Thumawadee Wongwirat[3], Guanchun Rui[3], Yingke Zhu[1], Daniel Hawthorne[2], Jiacheng Fan[1], Jianghan Wu[1], Siyu Zhang[1], Lei Zhu[*3], Sumanjeet Kaur[*2], and Qibing Pei[*1]

Operando Investigation of the Molecular Origins of Dipole Switching in P(VDF-TrFE-CFE) Terpolymer for Large Adiabatic Temperature Change

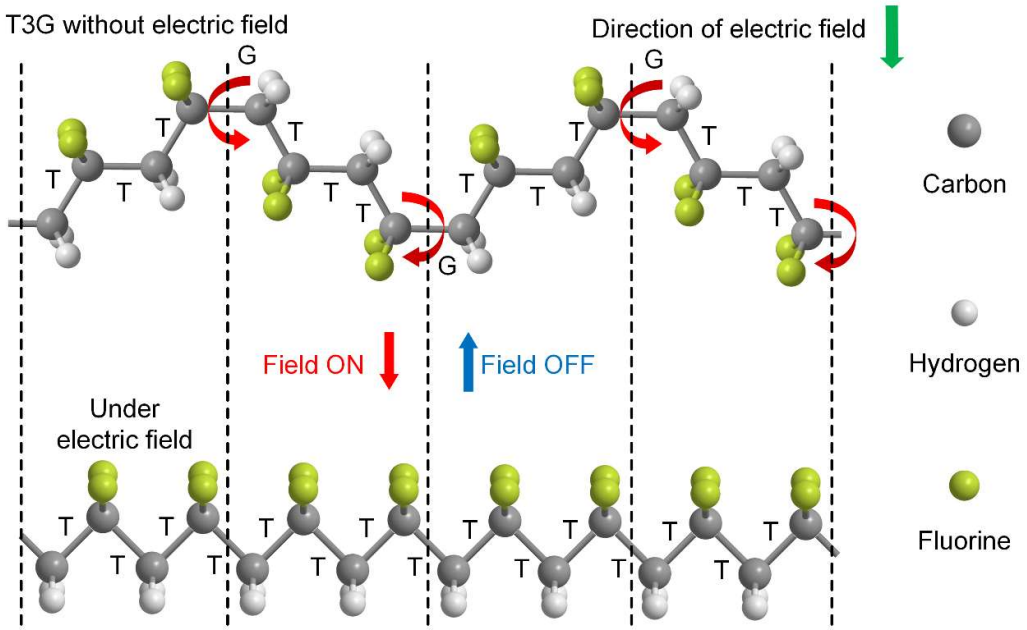

Supporting Information

Operando Investigation of the Molecular Origins of Dipole Switching in P(VDF-TrFE-CFE) Terpolymer for Large Adiabatic Temperature Change

*Yuan Zhu[†1], Hanxiang Wu[†1], Andrew Martin[2], Paige Beck[2], Elshad Allahyarov[3, 4, 5], Thumawadee Wongwirat[3], Guanchun Rui[3], Yingke Zhu[1], Daniel Hawthorne[2], Jiacheng Fan[1], Jianghan Wu[1], Siyu Zhang[1], Lei Zhu[*3], Sumanjeet Kaur[*2], and Qibing Pei[*1]*

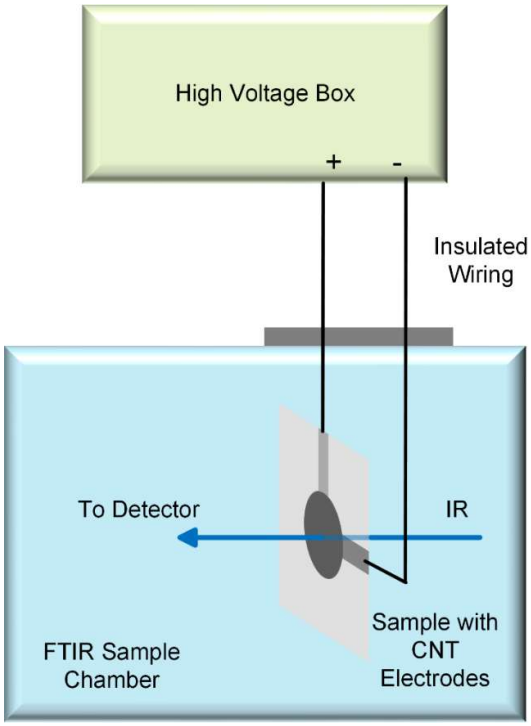

Figure S1. Operando FTIR set up. The direction of the applied electric field was parallel to the infrared light beam. Good insulation was achieved with insulating wires and tapes to prevent any shorting to happen.

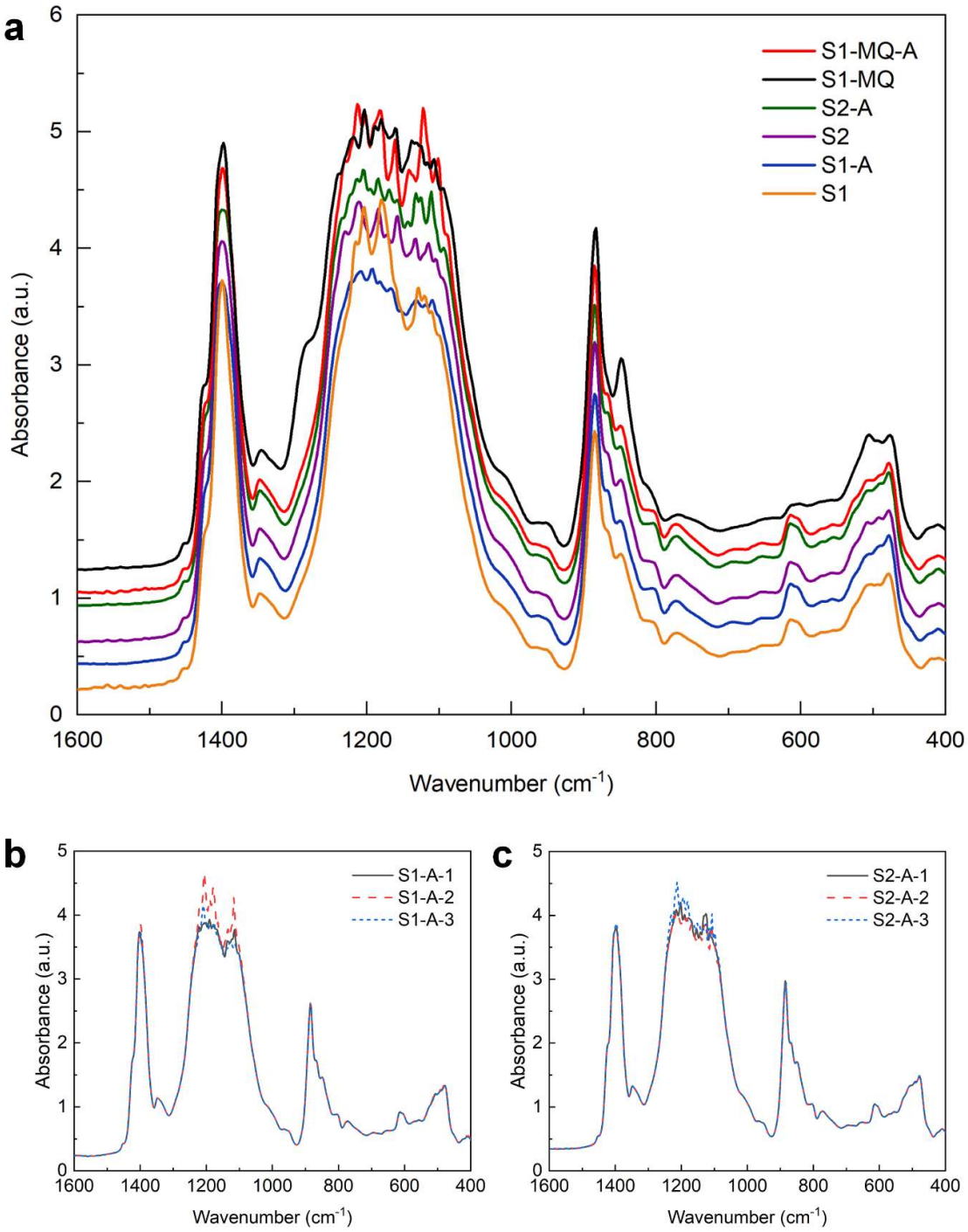

Figure S2. (a) Untruncated FTIR spectra of terpolymer films without electric field. Curves are elevated sequentially by 0.5 units in the vertical direction for easy reading purpose. (b) FTIR data without electric field of 3 different S1-A samples for reproducibility test. (c) FTIR data without electric field of 3 different S2-A samples for reproducibility test.

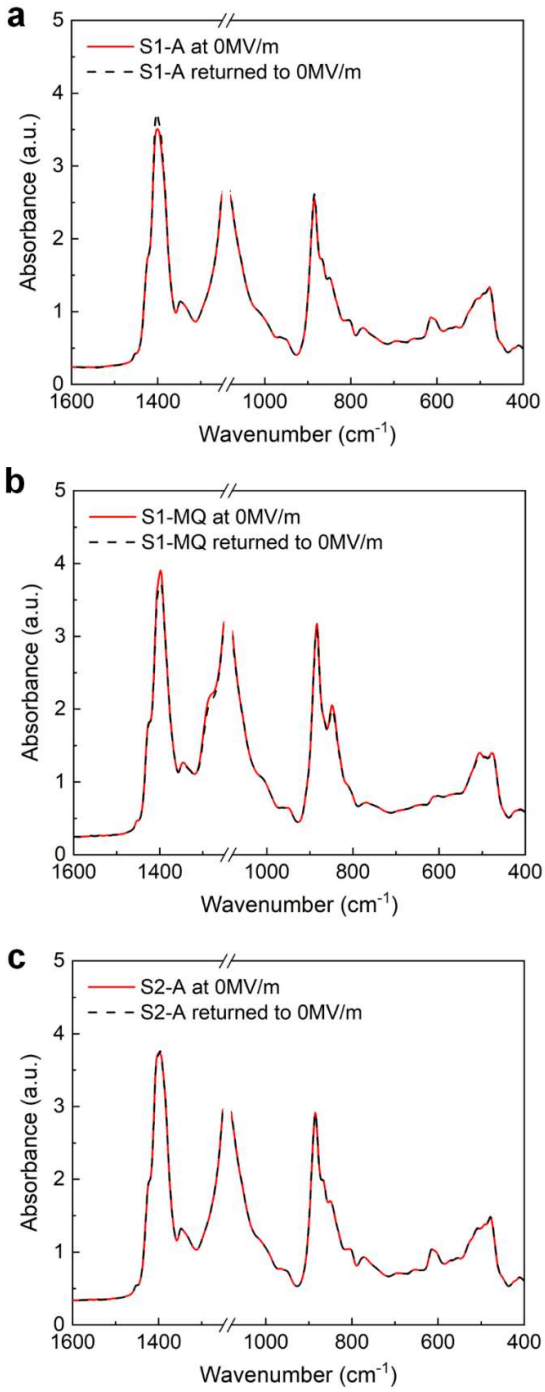

Figure S3. The FTIR spectra of the S1-A film (**a**), the S1-MQ film (**b**), and the S2-A film (**c**) before any electric field is applied (solid red curve), and at zero field after the sample has been subjected to a 20, 40 and 60 MV/m electric field (dashed black curve).

1. Molecular Dynamic (MD) Simulation

All the energies shown in Table S1 except the ΔU_{unit} were per atom and to get the total energy of the chain, one could simply multiply $U_{per\text{-}atom}$ by 95. The per-atom energy differences

between the four conformation chains and the long T sequence are noted as $\Delta U_{per\text{-}atom}$. When the energy differences between different conformation chains and the long T sequence was calculated, the contribution of the two TTT ends in each chain was regarded to be zero. Thus, to find this energy difference per chain, the $\Delta U_{per\text{-}atom}$ should be multiplied by 72. Here, 72 atoms were the chain atoms without the end TTT tails. Each tail had 11.5 atoms, and two ends had 23 atoms, thus 95 – 23 = 72. In the main text, we used the energy difference per TTTG, TGTG', or [(TTTG)(TGTG')]/2 unit to illustrate the ease of transformation from different conformations to a long T sequence. Since each repeating unit has 4 carbon-carbon bonds and 12 atoms in total, the energy difference between TTTG, TGTG', or [(TTTG)(TGTG')]/2 unit and the TTTT unit can be obtained by multiply $\Delta U_{per\text{-}atom}$ by 12.

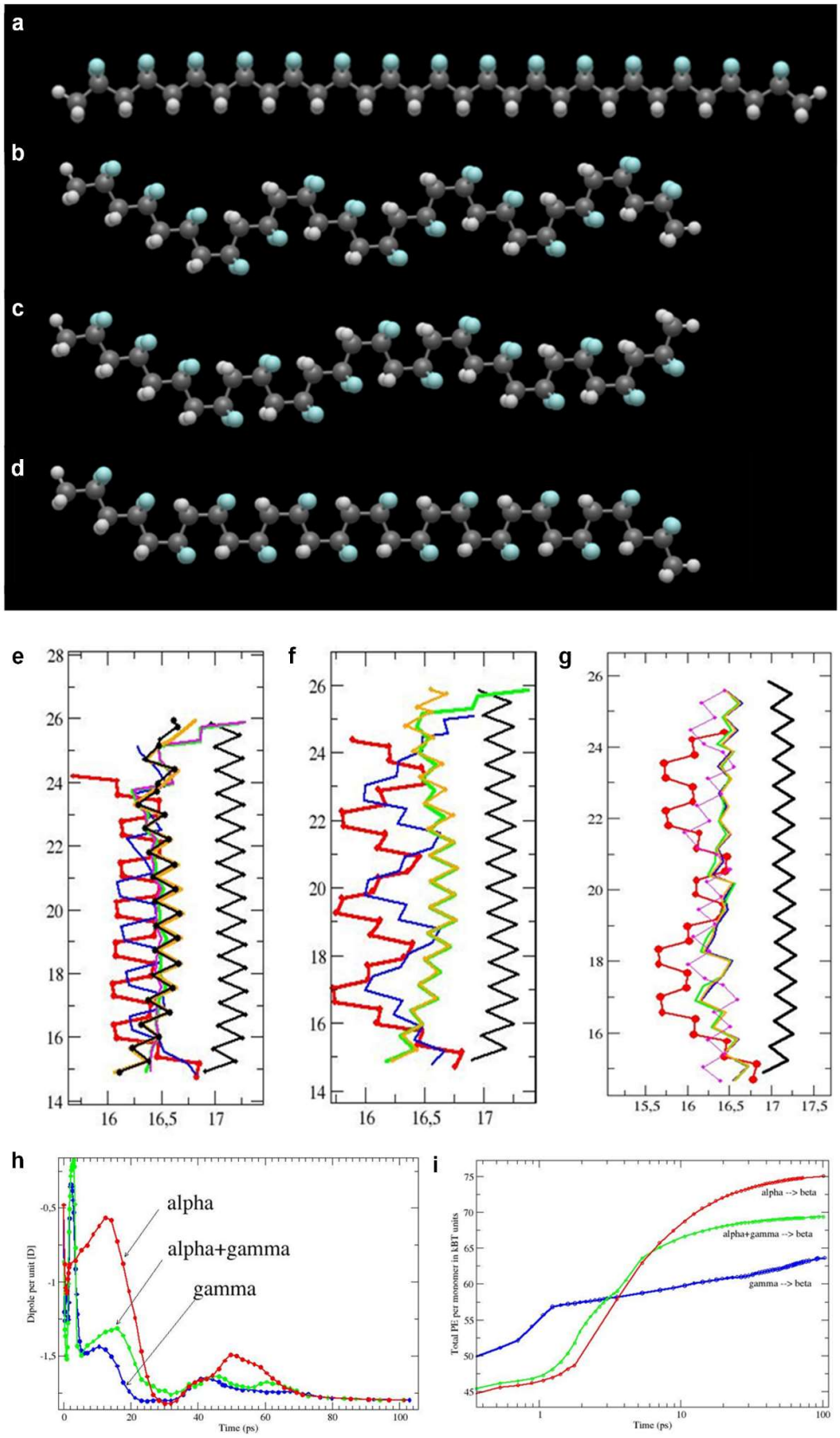

Figure S4. (**a**)-(**d**) Detailed configuration settings of conformations in molecular dynamics (MD) simulation of the long TTT(TTTT)$_6$TTT sequence (**a**), the γ-like conformation:

TTT(TTTG)$_6$TTT (**b**), the α-and-γ mixed conformation: TTT[(TTTG)(TGTG')]$_3$TTT (**c**), and the α-like conformation: TTT(TGTG')$_6$TTT (**d**). The carbon atoms are shown as dark-grey balls, the hydrogen atoms are shown as white balls and the fluorine atoms are shown as blue balls. (**e**)-(**g**) Representative snapshots taken at different simulation times *t* for the poled chains under the external field E = 100 MV m^{-1}. Only carbon atoms are shown. Black line on the right represents the β chain. (**e**) The α to β transformation: red line for t = 0 ps, blue line for t= 1.8 ps, green line for t=7 ps, pink line for t= 18 ps, orange line for t=30 ps, and black line with symbols for t= 60 ps. (**f**) The γ to β transformation: red line for t=0 ps, blue line for t= 1.8 ps, green line for t=30 ps, orange line for t=60 ps. (**g**) The α+γ to β transformation: red line for t=0 ps, pink line for t= 2.3 ps, blue line for t= 7.1 ps, green thin line for t=24.86 ps, and orange line for t=53.29 ps. (**h**) Changes in the dipole moment of the PVDF unit (CH2-CF2) during poling simulations as a function of the simulation time. It is evident that the γ chain is much faster to reaching (in absolute values) maximal dipole values at about 20 ps. (**i**) Potential energy (PE) per monomer (in k_BT units) during poling simulations as a function of time. It is evident that the γ chain needs a lower energy barrier for reaching the β phase.

Table S1. The calculated per-atom energies of the four characteristic conformation chains in MD simulation and the energy difference between TTTG, [TTTGTGTG']/2 and TGTG' repeating unit and the TTTT unit.

Conformation	**U_{coul} (eV)**	**U_{bond} (eV)**	**U_{angle} (eV)**	**$U_{torsion}$ (eV)**	**$U_{per-atom}$ (eV)**	**$\Delta U_{per-atom}$ (eV)**	**ΔU_{unit} (eV)**
long T sequence	0.366	0.028	0.114	0.084	0.590	0.000	0.000
γ-like chain	0.317	0.026	0.091	0.082	0.517	0.073	0.876
α-and-γ mixed chain	0.327	0.028	0.075	0.075	0.510	0.080	0.960
α-like chain	0.337	0.034	0.054	0.054	0.506	0.084	1.008

Table S2. Fusion enthalpy determined from the melting peak at 128 ºC on the DSC diagram (Figure S5). The temperature ramping rate was set to be 5 ºC min^{-1}. For S2* and S2*-A, the solvent evaporation temperature was 55 ºC.

Sample	Fusion Enthalpy ($J\ g^{-1}$)
S1	14.17
S2	20.05
S2*	17.40
S1-MQ	15.10
S1-A	19.57
S2-A	24.98
S2*-A	22.38
S1-MQ-A	17.98

Table S3. Peak locations and calculated inter-chain distances (d-spacing) in XRD spectra of the terpolymer films. The numerical values were generated by the built-in software (X'pert High Score Plus) of the XRD machine.

Sample	Paraelectric Peak Location (° of 2θ)	Paraelectric d-Spacing(Å)	Ferroelectric Peak Location (° of 2θ)	Ferroelectric d-Spacing(Å)
S1	18.46	4.81	19.54	4.54
S2	18.33	4.84	19.44	4.56
S1-MQ	18.54	4.79	19.44	4.59
S1-A	18.36	4.83	NA	NA
S2-A	18.28	4.85	NA	NA
S1-MQ-A	18.54	4.78	NA	NA

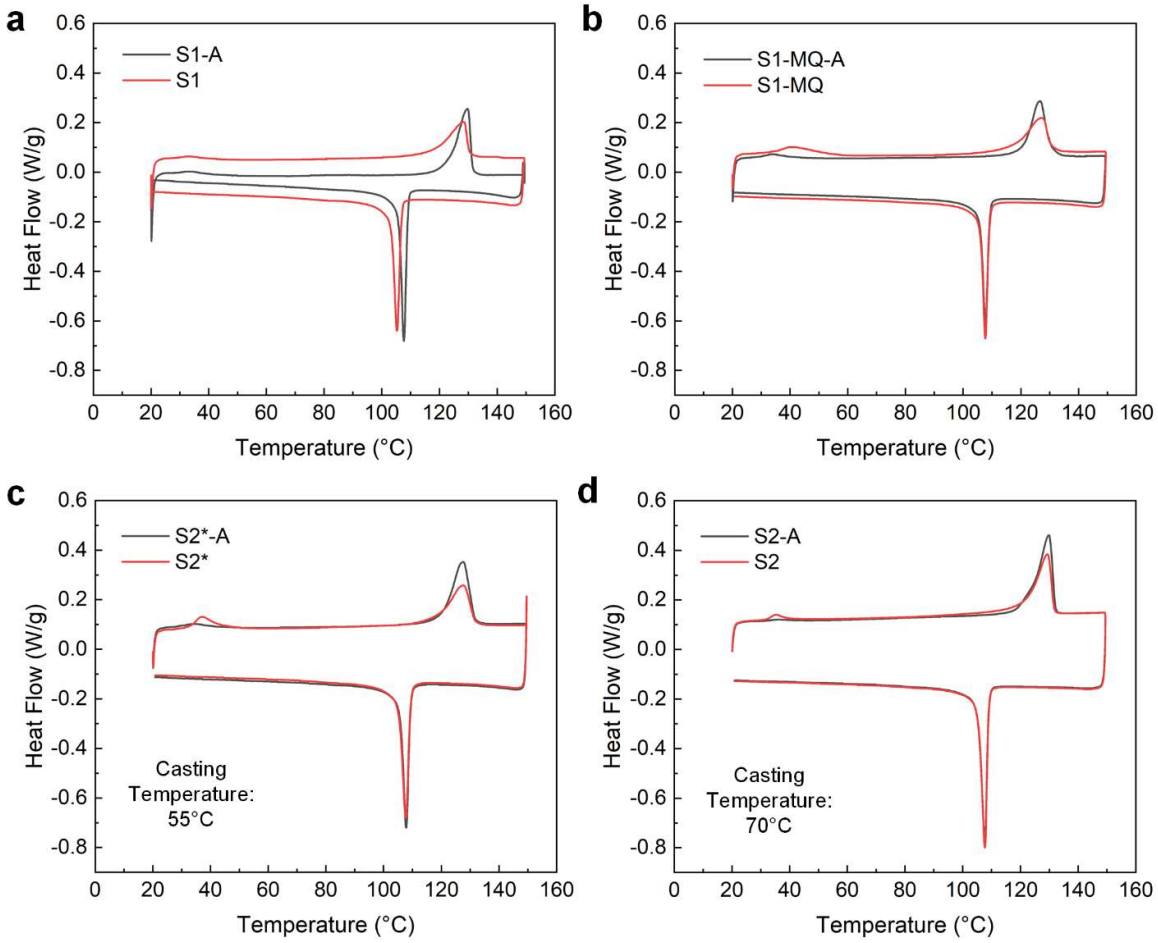

Figure S5. Differential scanning calorimeter (DSC) spectra of S1 and S1-A films (**a**), S1-MQ and S1-MQ-A films (**b**), S2* (cast at 55 ºC) and S2*-A films (**c**), and S2 (cast at 70 ºC) and S2-A films (**d**).

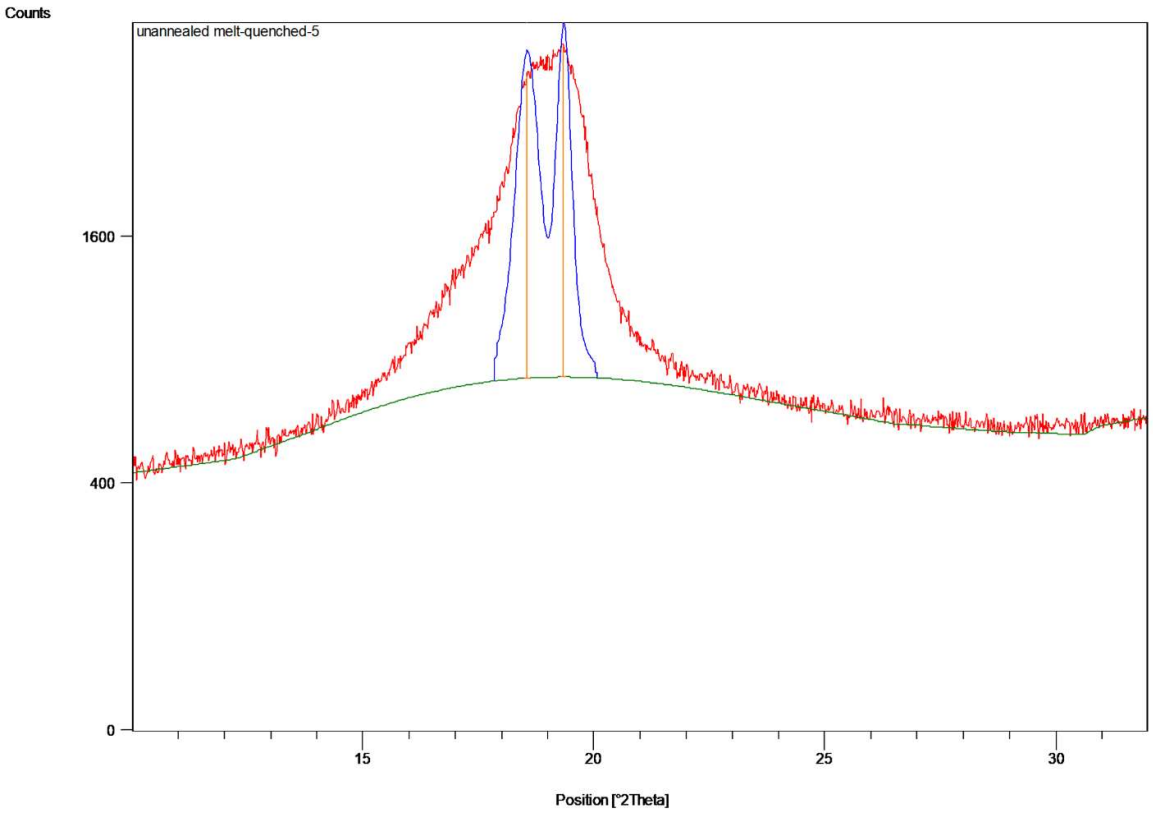

Figure S6. XRD peak of S1-MQ and the deconvolution of the wide diffusive peak into a paraelectric phase peak and a ferroelectric peak using the X'Pert High Score Plus software.

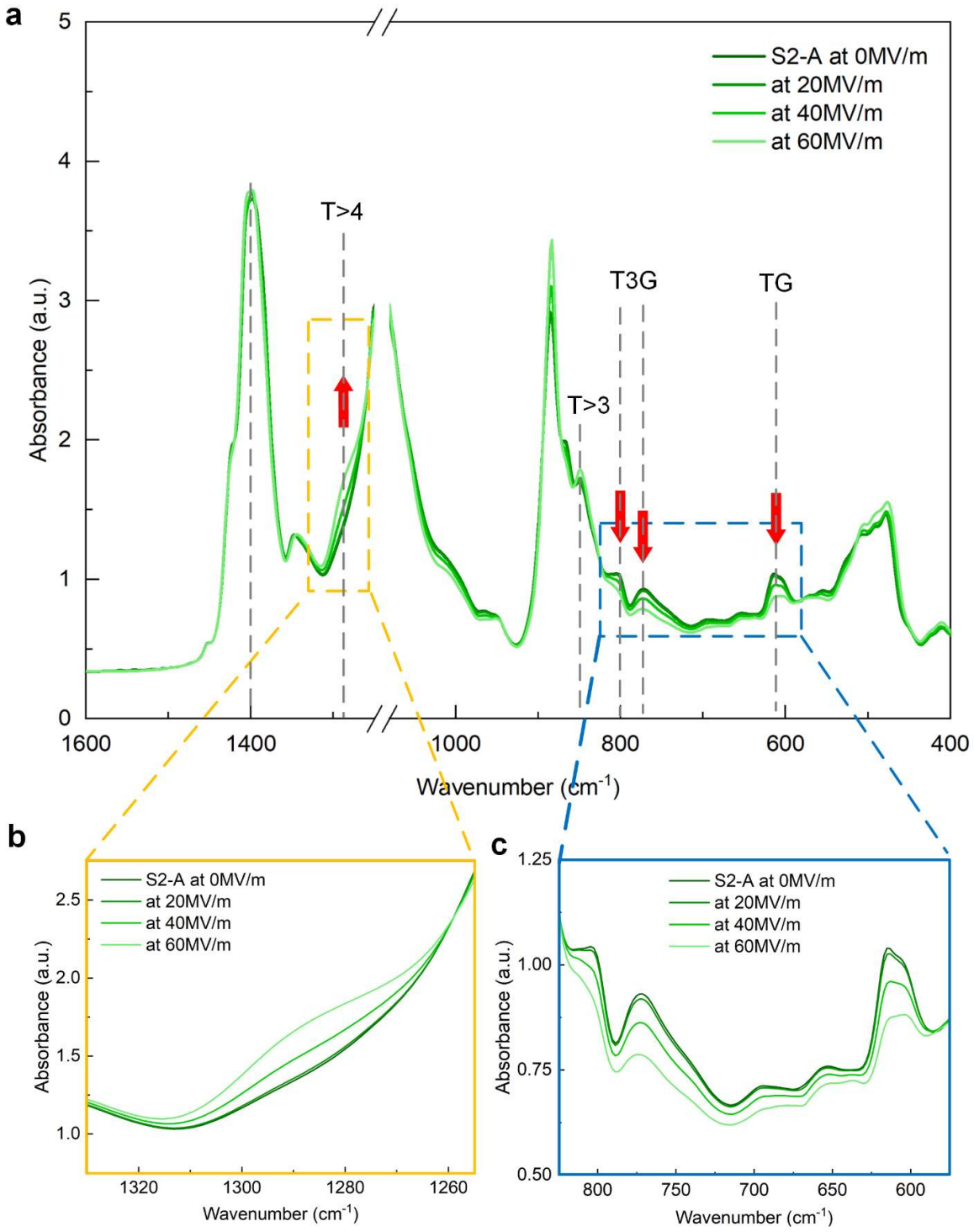

Figure S7. (**a**) Operando FTIR spectra of the S2-A that contains a large number of T3G sequences. Detailed views of the spectral changes of long T sequences (T>3) around 1287 cm^{-1} (**b**) and T3G at 772 and 800 cm^{-1} plus TGs in short T sequences at 605/614 cm^{-1} (**c**).

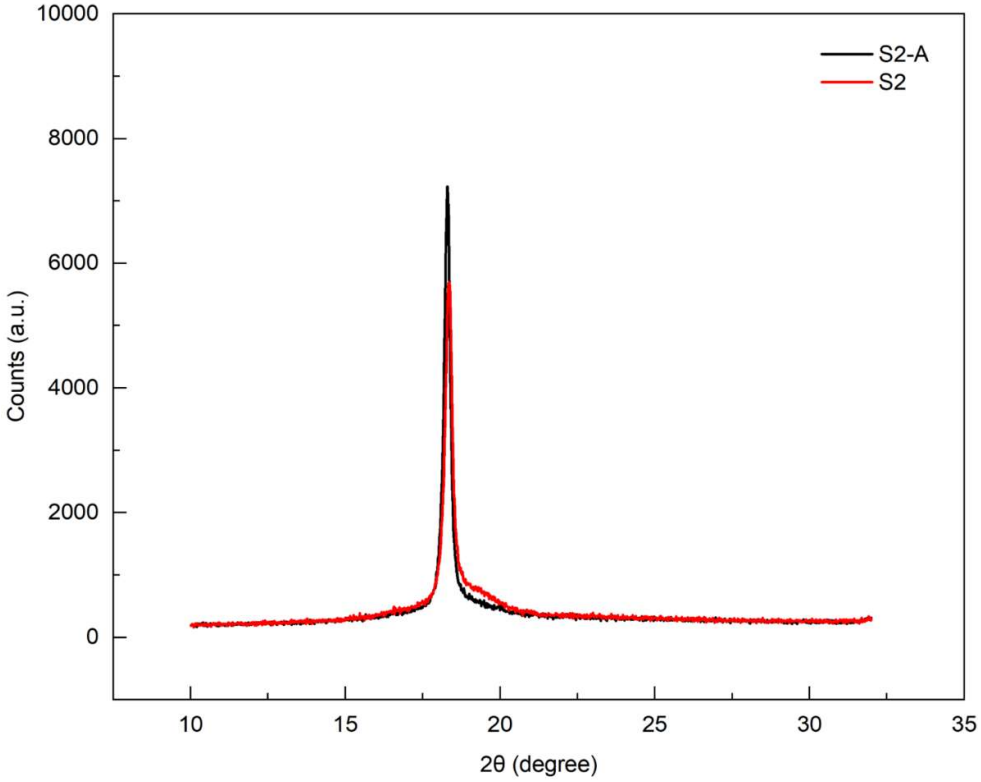

Figure S8. XRD spectra of S2 and S2-A samples.

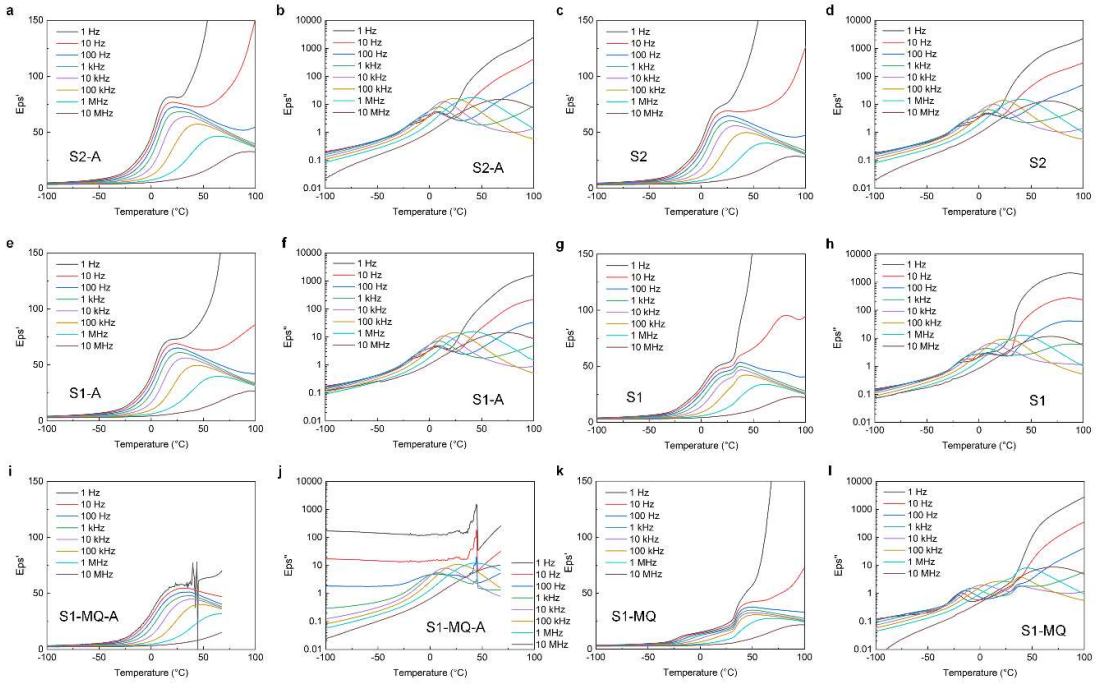

Figure S9. Temperature-scan BDS data for the real and imaginary relative permittivity of sample S2-A (**a**-**b**), S2 (**c**-**d**), S1-A (**e**-**f**), S1 (**g**-**h**), S1-MQ-A (**i**-**j**), S1-MQ (**k**-**l**), respectively.

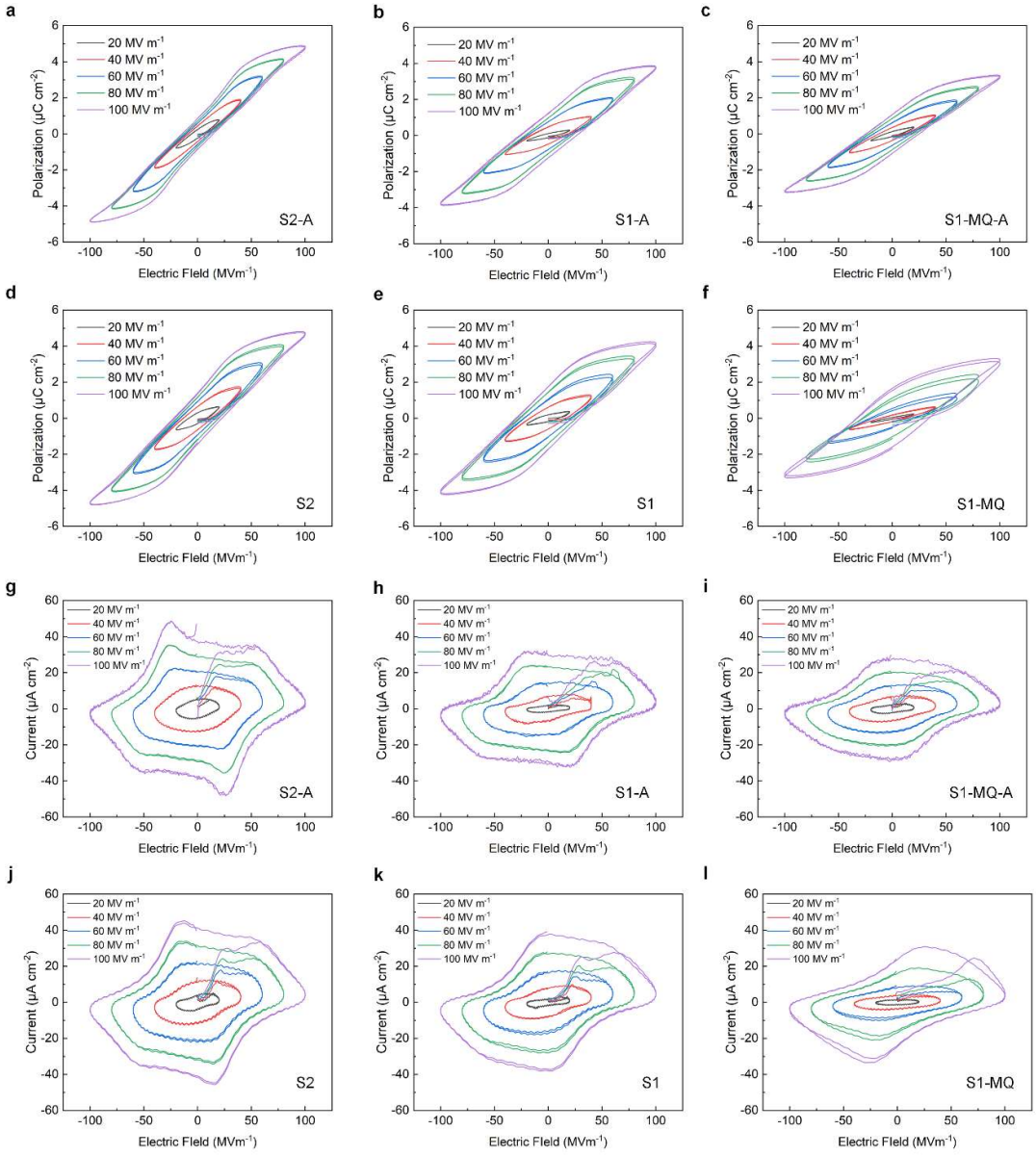

Figure S10. D-E loop of sample S2-A (**a**), S1-A (**b**), S1-MQ-A (**c**), S2 (**d**), S1 (**e**), and S1-MQ (**f**), at 1Hz respectively. I-E loop of sample S2-A (**g**), S1-A (**h**), S1-MQ-A (**i**), S2 (**j**), S1 (**k**), S1-MQ (**l**), at 1Hz respectively.